Optimal Algorithmic Techniques of LASIK Procedures

A thesis submitted in fulfillment of the requirements
for the award of the degree of

Master of Philosophy

by

Fan Yi
BEng

from

School of Engineering
Faculty of Engineering and Information Technology

GRIFFITH UNIVERSITY
GOLD COAST CAMPUS

October 2005

Declaration

This work has not been previously submitted for a degree or diploma in any university. To the best of my knowledge and belief, the thesis contains no material previously published or written by another person except where due to reference is made in the thesis itself.

_____

Fan Yi

October 2005

List of Publications

The following publication is related to this thesis topic:

Journal paper:

Yi F, Iskander DR, Franklin R and Collins MJ (2006). "Computer simulation of visual outcomes of wavefront-only corneal ablation." J Cataract Refract Surg **32**: 487-494

Abstract

Clinical wavefront-guided corneal ablation has been now the most technologically advanced method to reduce the dependence of glasses and contact lenses. It has the potential not only to eliminate spherocylindrical errors but also to reduce higher-order aberrations (HOA). Recent statistics show that more than 96% of the patients who received laser in situ keratomileusis (LASIK) treatment reported their satisfaction about the improvement on vision, six months after the surgery. However, there are still patients complaining that their vision performance did not achieve the expectation or was even worse than before surgery. The reasons causing the unexpected post-surgical outcome include undercorrection, overcorrection, induced HOA, and other postoperative diseases, most of which are caused by inaccurate ablation besides other pathological factors. Therefore, to find out the method to optimize the LASIK procedures and provide a higher surgical precision has become increasingly important. A proper method to calculate ablation profile and an effective way to control the laser beam size and shape are key aspects in this research to resolve the problem.

Here in this Master of Philosophy degree thesis, the author has performed a meticulous study on the existing methods of ablation profile calculation and investigated the efficiency of wavefront only ablation by a computer simulation applying real patient data. Finally, the concept of a refractive surgery system with dynamical beam shaping function is sketched, which can theoretically overcome the disadvantages of traditional procedures with a finite laser beam size.

Keywords: Higher-order aberration, refractive error, LASIK, beam shaping, corneal ablation, wavefront

Acknowledgements

I would like to thank all the people who have assisted me through the preparation and completion of this thesis. In particular, I sincerely wish to express my gratitude and appreciation to my supervisors, Dr. D. Robert Iskander and Khoa N. Le, who have guided me from the commencement to the successful completion of my study. Without their guidance and encouragement, I would not have been able to reach this point.

To Dr. Charles Hacker, who was my associate supervisor, my thanks for his valuable comments on my confirmation seminar.

To Dr Tobia Buehren, Dr Ross Franklin and Dr Michael J. Collins, at the Queensland University of Technology, my thanks for their help in collecting all the real patient data in this study, reading of the Journal paper and useful comments.

To my friends, Mr Dong-Jun Lee, Mr Daeho Cha, Mr Nathan Benfer, Mr Giuseppe Cirella, Mr Ryan Dunn, Mr Luke Menefy and Mr Chris Scraggs, thanks for their giving me a lot of happy memory during the project.

Specially thanks to Miss Xiao-Dan Wang for giving me a lot of support during my study.

Finally and foremost, I would like to thank my parents, who support me to study in Australia financially and emotionally.

Contents

Declaration i

List of Publications ii

Abstract iii

Acknowledgements iv

List of Figures vii

List of Tables ix

List of Symbols x

1 Introduction 1

1.1 Background 1

1.2 Objectives 2

1.3 Outline of the thesis 2

2 Introduction to technological aspects of modern refractive surgeries 4

2.1 Optical characteristics of the human eye 4

2.1.1 Refractive theory and visual errors 4

2.1.2 Measurement of corneal topography 8

2.1.3 Wavefront sensing 9

2.1.4 Ray-trace technology 13

2.1.5 Modeling wavefront data with Zernike polynomials 16

2.2 Modern refractive surgeries 17

2.2.1 Principle of clinical laser vision correction 17

2.2.2 LASIK procedures 21

3 Ablation Profile Calculation 24

3.1 Approximated Munnerlyn formula 24

3.2 Ablation profiles for wavefront optimized corneal correction 27

3.2.1 Klein's wavefront only approximation 28

3.2.2 Mrochen *et al.*'s wavefront optimized ablation method 32

3.2.3 Manns et al.'s algorithm 34
3.3 Future development of algorithms calculating ablation profiles 36

4 A Comparison of Ablation Profile Methods 38

5 Evaluation of the Wavefront Only Corneal Ablation 45
5.1 Subjects and Methods 46
5.2 Computer simulation 48
5.3 Data analysis 51
5.4 Results 55
5.4.1 RMS of wavefront aberration 55
5.4.2 Visual Strehl ratios (VSOTF) 55
5.4.3 Effect of decentration in surgical outcome 57
5.5 Summary 59

6 Potential Technologies of the Future 63
6.1 Design of an advanced laser scanning algorithm 63
6.1.1 Manns et al.'s scanning algorithm for corneal reshaping 64
6.1.2 Adjustment factor to compensate the energy loss at periphery area due to reflection and decrease of energy density 67
6.1.3 Correction factor of overlap with Gaussian-profile beams 72
6.2 Technologies of real time laser beam shaping 74
6.2.1 Beam shaping by using optical displacement elements 75
6.2.2 Multi-spots technique 77
6.2.3 Beam shaping by using digital mirror devices 77
6.3 Concept of a refractive surgery system adopting digital mirror device as the beam shaping and delivery subsystem 80

7 Conclusions and Recommendations 85

References 87

Appendix 1 98

List of Figures

2.1 Optical paths in a simplified emmetropic eye. 5

2.2 In eyes with myopia (shortsightedness), rays of light focus in front of the retina. 6

2.3 In hyperopia (farsightedness), rays focus behind the retina. 6

2.4 Light focuses multiple areas in astigmatism. 6

2.5 An example of an E letter image in eyes with irregular astigmatism. 7

2.6 The format of output files from the Keratron videokeratoscope. 9

2.7 OPD for positive aberration. 11

2.8 The modern aberrometer built on the Scheiner-Hartmann-Shack principle. 12

2.9 Grid pattern of (a) the ideal wavefront, and of (b) aberrated wavefront. 13

2.10 Ray tracing in 2-D. 15

2.11 Ray tracing in 3-D. 15

2.12 The stages of photoablation process. 20

3.1 Ablation depth for spherical Myopia. 25

3.2 HS sensors measuring aberrations from the eye. 29

3.3 Ablation pattern for myopia. 31

3.4 Ablation pattern for hyperopia. 31

3.5 The three steps in Mrochen *et al*. formula (a) Measure and map total wavefront. (b) Inverse the wavefront map. (c) Converse wavefront to ablation depth 33

5.1 Flow chart of computer simulation procedures. 48

5.2 Pupil Offset Adjustment. 49

5.3 Simulated impact of different aberrations on the vision performance. 53

5.4 (a) MTF of Eye1. (b) MTF of Eye2. 54

5.5 Pre- and “post”-operative wavefront RMS for total (left) and higher order 56

(right) aberrations. The ablation procedure uses only total eye wavefront data (no corneal topography information) and assumes perfect ablation.
5.6 Pre- and "post"-operative VSOTF based on higher-order aberrations only and assuming perfect ablation. 56
5.7 VK pupil offset with an additional 150 μm decentration in θ direction. 57
5.8 Pre- and "post"-operative wavefront RMS for total (left) and higher order (right) aberrations. The ablation procedure uses only total eye wavefront data (no corneal topography information) and assumes ablation misalignment of 150 μm. 58
5.9 Pre- and "post"-operative VSOTF based on higher-order aberrations only and assuming ablation misalignment of 150 μm. 58

6.1 Algorithm for the calculation of the pulse-distribution map. 65
6.2 Schematic representation of a non-normal incident laser beam. 70
6.3 Effective illumination area on the corneal curvature surface. 70
6.4 Effect of overlapping due to finite-size of the incident beam. 74
6.5 Increase of energy losses at periphery area using fixed beam size laser. 75
6.6 Structure of the optical displacement sensor. 76
6.7 Optics of the optical displacement sensor. 76
6.8 An approximated elliptical spot composed by 7 spots. 77
6.9 Configuration of the Micro-mirror. 78
6.10 Optics of a Micro-mirror. 78
6.11 A DMD panel working on reflecting mode, the circle stands for the diameter of the laser beam. 80
6.12 Proposed wavefront based refractive surgery system with the beam shaping and delivery subsystem utilizing DMD. 82
6.13 DMD beam shaping for a pre-calculated ablation profile from wavefront. 83

List of Tables

2.1 Absorption rates of ocular refractive components to different wavelength of a laser beam. 19

3.1 Parameters of the Navarro model of the relaxed eye. 35

4.1 A comparison of ablation profile methods 44

5.1 The subjects used in the study. 47

List of Symbols

A_{eff}	Effective illumination area
$CSF_N(f_x, f_y)$	Neural contrast sensitivity function
D	Diopters
D_1	Amount of removal in diopters
D_A	Ablation depth by approximated Munnerlyn formula
D_{c-A}	Ablation depth by Klein's approximation
D_{th}	Ablation depth by Munnerlyn's formula
E	Location of reference plane
F	Incident exposure of the laser beam
I_0	Maximum radiant exposure
I_p	Plateau radiant exposure
I_{th}	Ablation threshold
N	Number of required pulses
OPD	Optical path difference
OPL	Optical path length
$OTF_{DL}(f_x, f_y)$	Diffraction limited optical transfer function
OZ	Radius of ablation zone
P	Normalized distance from the origin
P_f	Final paraxial power of the anterior corneal surface
P_i	Initial paraxial power of the anterior corneal surface
Q_f	Asphericity factor
Q_p	Parallel polarization amplitude coefficients of reflection
Q_s	Sagittal polarization amplitude coefficients of reflection
R_1	Initial radius of corneal curvature
R_2	Final radius of corneal curvature
S	Sagittal depth
S_A	Approximated sagittal depth
V	Ablation volume
W_1	Contribution of anterior corneal surface to the spherical aberration

W_2, W_3, W_4	Aberration coefficients of the posterior corneal surface, anterior lens surface and posterior lens surface
$W(\rho,\theta)$	Wavefront aberration
$Z_p\ (\rho,\theta)$	pth Zernike polynomial
Z (x,y)	Corneal topography
a_p	Coefficient associated with $Z_p(\rho,\theta)$
b	$1/e^2$ diameter of the Gaussian beam
c	Correction factor of laser beam overlap
d	Distance from HS plane to corneal vertex
d_p	Ablation depth per pulse
h	Planck constant (=6.626×10^{-34} J.S)
k_1	Compensation factor of non-normal incidence
k_2	Compensation factor of reflection
m	Ablation rate at $F = e \cdot F_{th}$
n	Refractive index
Δn	Difference of refractive index
p	Polynomial-ordering number (=1, 2….P)
r	Radius
$refl(r)$	Reflectivity at a point with a radial distance r from the corneal apex
x, y, z	Cartesian co-ordinates
α	Incident angle
α'	Diffractive angle
θ	Angle
$\Delta\theta$	$\pi/128$
ε	Energy of photons
$e(\rho,\theta)$	Measurement and modeling error (noise)
λ	Wavelength
∞	Infinite far distance

Chapter 1

Introduction

1.1 Background

Laser vision correction is the most technologically advanced method available today to reduce the dependence on glasses and contact lenses. The first step of laser refractive surgery occurred in 1980 when Beckman and Peyman and their associates used a carbon dioxide laser in the experiment to create thermal shrinkage of the cornea in order to change corneal contour (Xu, 1995). Then, in 1981 the discovery reported by John Taboada showed that the argon-fluoride excimer laser had the ability to indent surface epithelial corneal tissue (Li and Zhu, 2001). After the development of photorefractive keratectomy (PRK) during the period from 1985 to late 1990s, Laser in situ keratomileusis (LASIK) brought an evolution to the application of laser technology to vision correction, and became presently the most commonly performed laser vision correction technique among all the refractive surgeries using excimer laser. There are millions of patients receiving laser corneal surgery through out the world every year, and the number is growing daily (Brunette *et al*., 2000; Terry, 2000).

With a goal to provide better vision performance and reduce the dependency on eyeglasses and contact lenses, LASIK surgery has a satisfied result in eliminating some aberrations such as defocus and astigmatism. However, some problems with the procedure like the pre-determined method of laser pulse delivery including the pre-determined beam shape and size as well as the method of calculating ablation profile limit the surgical performance on treating complex aberrations and sometimes cause unexpected post-surgical outcomes, which are due to inaccurate ablation, such as halos, glare disability, and night-vision disturbances (Bailey and Mitchell, 2001;

Miller *et al.*, 2001). Therefore, the importance of finding the solution to improve the current LASIK procedure becomes increasingly obvious.

1.2 Objectives

In the area of research to optimize the LASIK process, only a few works have been done. Most of them are focusing on analysis of the relation between laser beam size and shape and the ablation result by using now available laser systems and integrated software. The author's research study aims to develop the methodology improving the working method of current LASIK technology to achieve a higher surgical precision, thereby to insure the least amount tissue removed while providing an optimized ablation result. Major objectives include:

- Find out the effective algorithm for calculating the ablation pattern of comprehensive wavefront-guided corneal correction
- Develop a computer program to simulate the ablation process based on the above ablation pattern algorithm
- Apply real patient data in the computerized simulation to examine the effectiveness of proposed algorithm
- Disseminate the knowledge required in this study to wider engineering and ophthalmology communities

1.3 Outline of the thesis

The optimization of current LASIK procedures is a complex problem including the aspects of algorithm and system hardware. In this study, solutions improving the performance of LASIK technology are proposed.

Following the introduction in Chapter 1, technological aspects of modern Laser refractive surgery will be reviewed and disadvantages of current LASIK technology will be summarized in Chapter 2. Then, in Chapter 3, different algorithms calculating the ablation profile, which is one of the most important factors affecting the surgical

precision, will be discussed. A detailed comparison of ablation profile methods reviewed is included in Chapter 4, and Klein's wavefront-only approximation (Klein, 1998) is selected for following simulation study.

Based on the algorithm calculating ablation profiles utilizing only wavefront data, a computer simulation program is designed. Additionally, the simulated surgical results will also be shown in Chapter 5.

Finally, new technologies with the potential to improve the current LASIK procedures both on software and hardware are introduced in Chapter 6, and a system concept with the potential for comprehensive wavefront aberration correction is sketched. One of the important features of the system is the adoption of digital mirror device (DMD) as the beam shaping and delivery subsystem. The conclusions and recommendations of the present research study are given in Chapter 7.

Chapter 2

Introduction to technological aspects of modern refractive surgeries

2.1 Optical characteristics of the human eye and measurement

As a first approximation, optical components of the human eye work together much like a camera. Refractive materials including cornea, aqueous in the anterior chamber and crystalline lens, compose the camera lens. Pupil acts as the diaphragm, and retina is taking the place of film. The total optical power of the human eye is close to 60 D (diopters) in a relaxed state. When it reaches the maximum adjusting power, the value will increase to about 70 D (Xu, 1995). With such a flexible high refractive power system, the human eye can achieve precise imaging functions and bring clear images to the retina.

2.1.1 Refractive theory and visual errors

One of the basic requirements for the human eye to obtain clear images from the object is that image of the object is formed on the retina with a proper resolution, which requires accurate cooperation between all the refractive components (Xu, 1995). A simplified eye model is adopted to describe various cases of incident light focusing as shown in Figure 2.1.

The cornea is the major refractive component in the human eye. It contains approximately two thirds of the eye's optical power (Artal and Guirao, 1998;

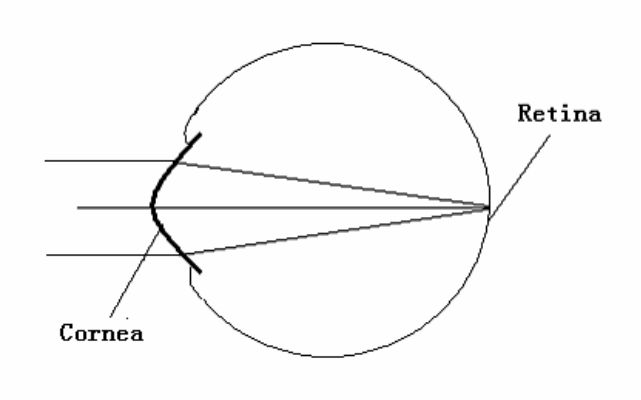

Figure 2.1 Optical paths in a simplified emmetropic eye.

Courville *et al*., 2003). In the ocular system, it is the front-most surface and acts as a convex lens bending and refracting the light that passes through the cornea. An ideal condition is that the transmission light should be correctly focused onto the retina to produce a clear image. However, the irregularity of the corneal surface affects the precision of optical path and causes a series of focusing fault stands for different refractive errors.

Aberrations (Refractive Errors)

Refractive errors refer to disorders of light focusing in the eye. They are classified into conventional aberrations and higher order aberrations.

i) Defocus

Defocus occurs when the eye is functionally too long or too short for the focusing power of the cornea and lens.

When the curvature of cornea is considered too steep comparing to the length of eye, even if the corneal shape is perfect, light rays passing the cornea will focus in front of the retina causing a blurred image. This case is called myopia, which is displayed in Figure 2.2.

Being opposite to myopia, in eyes with hyperopia, light rays can only focus behind the retina as shown in Figure 2.3. This situation also produces a blurred image.

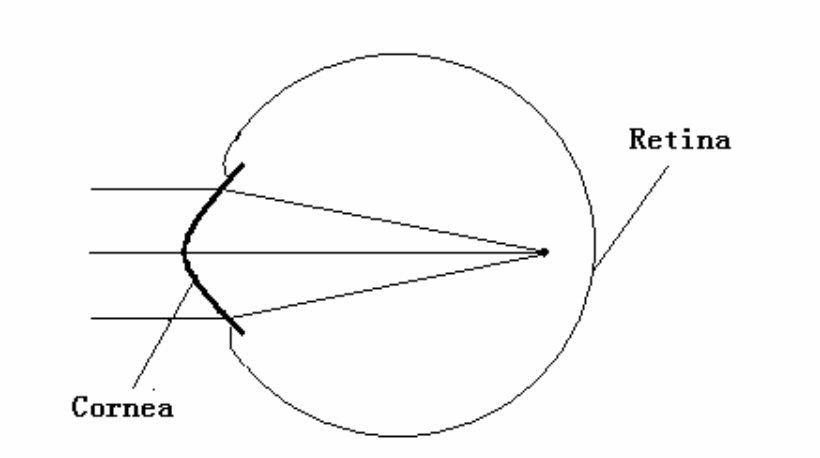

Figure 2.2 In eyes with myopia (shortsightedness), rays of light focus in front of the retina.

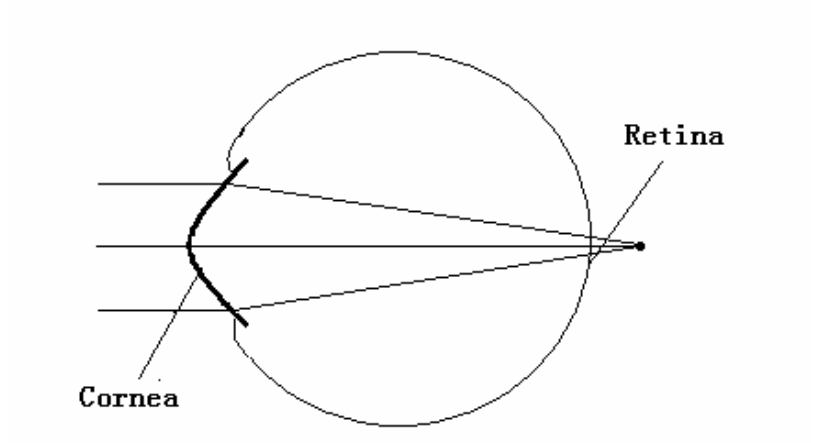

Figure 2.3 In hyperopia (farsightedness), rays focus behind the retina.

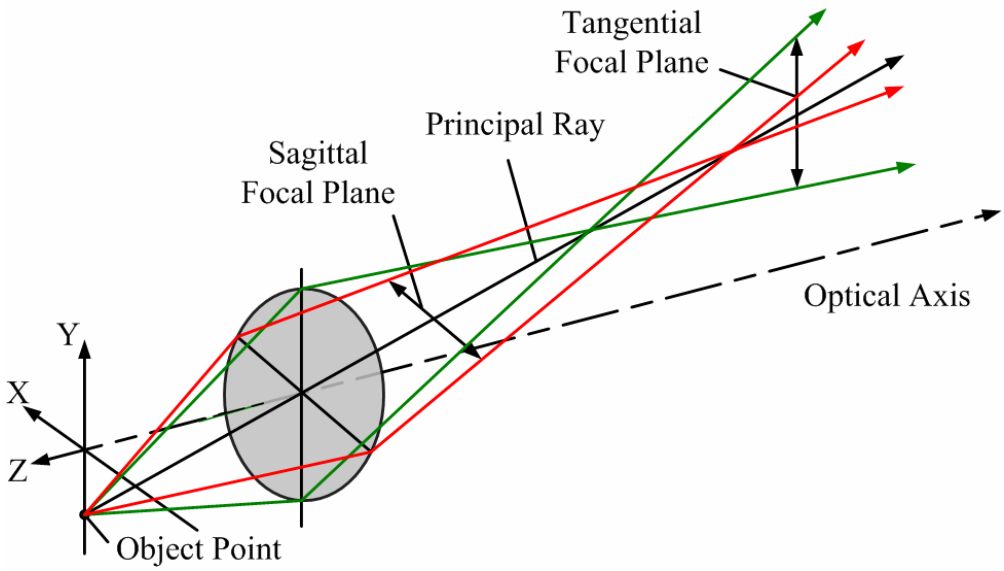

Figure 2.4 Light focuses multiple areas in astigmatism.

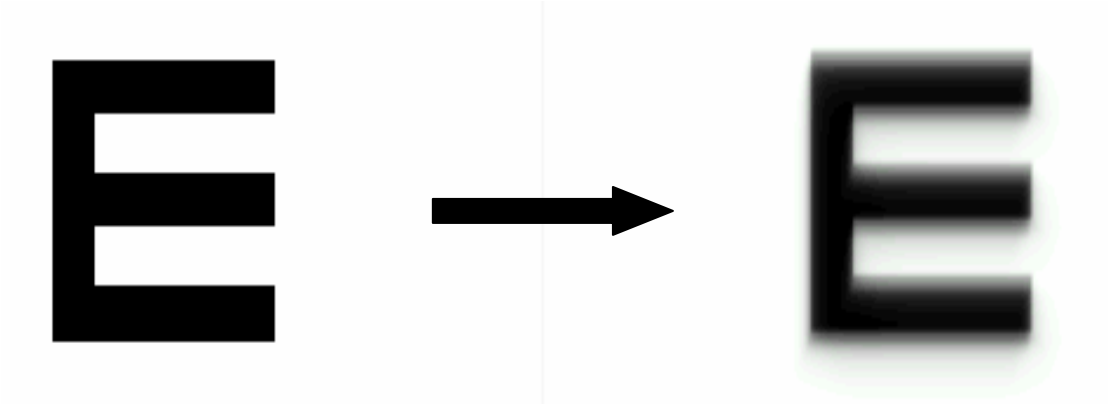

Figure 2.5 An example of an E letter image in eyes with irregular astigmatism.

ii) Astigmatism

The cornea with astigmatism can be approximated by ellipsoid or ovaloid without rotational symmetry. Generally, the refractive power on the tangential focal plane is greater than the sagittal plane, which causes focusing error, as shown in Figure 2.4, .

iii) Irregular astigmatism (higher order aberration)

Irregular astigmatism refers to aberrations, which are not accounted by defocus and astigmatism. In most of human eyes, this part of aberration only accounts to a small percentage of the total amount of vision error. Without having an obvious effect on image as the conventional aberrations, irregular astigmatism also decreases the quality of the retinal image. As represented in Figure 2.5, the letter E displayed in the eye with irregular astigmatism is blurred from the original.

If the considered aberrations are minimized, image contrast and sharpness for special detail will be increased. Particular benefit to individuals with unusually large amounts of higher-order aberrations would also be achievable.

Several technologies, which are now important aid in modern refractive surgery, will be introduced in the following section.

2.1.2 Measurement of corneal topography (videokeratoscopy)

The anterior surface of the cornea contributes about 48.8 D of the refractive power compared to 58.64 D of the whole eye (Xu, 1995). Even very minor distortions in the shape of the cornea can seriously degrade the visual acuity (Dave, 1998; Courville *et al.*, 2003). Therefore, measurement of its shape has an important role in various optometric and ophthalmological procedures including refractive surgery. Furthermore, study of sequential changes of corneal topography with time is important in monitoring long-term postoperative outcome (Chuck *et al.*, 2001; Erie *et al.*, 2004).

A widely used instrument for measuring corneal topography is a videokeratoscope. It calculates corneal height, axial power and surface curvature from a CCD image of a set of alternating concentric rings of light and dark, called Placido rings (Doss *et al*., 1981), reflected from the cornea.

In all Placido devices, the cornea acts like a mirror. Light reflected from a luminous ring off the cornea is assumed to focus on the same focal plane (Rand *et al.*, 1997). To completely determine the corneal shape, the x, y (the x, y information is usually converted to r, θ in polar coordinates), and z location of every point on the corneal surface must be measured. However, videokeratoscopes only record two-dimensional images of the Placido-rings reflected from the cornea. Therefore, different corneal models and algorithms are adopted to calculate the corneal shape. An arc-step algorithm (Mattioli and Tripoli, 1997), a surface reconstruction method that is not spherically biased, is adopted by Keratron videokeratoscopes, which are used in this study to collect the real corneal data from patients.

The output data from the Keratron videokeratoscope is used in the author's MPhil study. The data points on the cornea are sampled in a ring pattern composed of 26 concentric rings. For each measurement, two text files are output for the radial and z-coordinate, which is recorded in format shown in Figure 2.6.

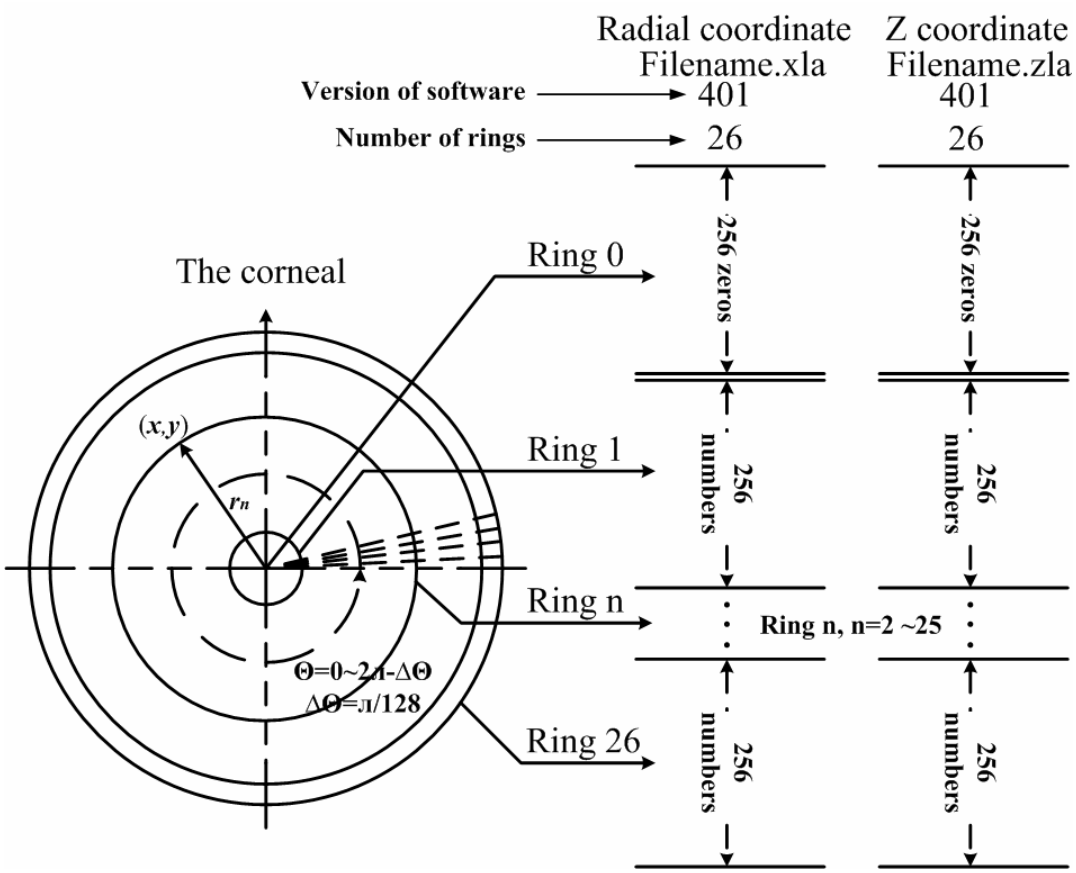

Figure 2.6 The format of output files from the Keratron videokeratoscope.

There are 256 equidistant points on each ring taking an increment of π/128 from 0 to 2π-π/128. For this reason, there is no output file for angular information. Points with the same angular coordinate lie on a radial line on the cornea compose a semi-meridian. The plane containing the *z*-axis and a semi-meridian is called as the meridional plane at a particular angle.

2.1.3 Wavefront sensing

Since the introduction of advanced wavefront sensing technologies, there is now a powerful adjunct for clinicians and optometric researchers to precisely measure the whole-eye wavefront aberration and determine the interplay between the corneal surface and intraocular components, especially the lens. It is one of the main forces leading to an innovation in refractive surgery, which is wavefront-guided corneal correction.

To define the concept of wavefront aberration, it is necessary to define the wavefront from a point light source, and before that, the concepts of optical path length (*OPL*) and optical path difference (*OPD*).

From a clinical perspective, the most frequently used explanation for wavefront aberration is by errors of the optical path length (*OPL*). The optical path length specifies the number of times a light wave needs to oscillate traveling from point A to another point B. It is defined mathematically as integration of the refractive index with respect to the distance along the ray path from A to B (Applegate *et al*., 2001).

$$OPL = \int_A^B n(s)ds \tag{2-1}$$

If the light ray is traveling in homogenous materials, it becomes the sum of distance traveled in each material multiplied by the refractive index of that material.

$$OPL = \sum_{i=1}^{m} n_i \cdot s_i \tag{2-2}$$

For air-cornea ray paths, the *OPL* can be simply calculated by

$$OPL = s_1 n + s_2 n' \tag{2-3}$$

Where n and n' are refractive indexes of air and cornea respectively. Since the propagating speed of light is slower in optically denser media, more oscillations will occur in the eye than with the same physical distance in air. By defining the *OPL* as the product of the physical path length with the refractive index, *OPL* becomes a measure of the numbers of oscillations undergone by a propagating light ray. Although the light rays from a point source are emitted in different directions, they have the same *OPL* at any instant in time.

The wavefront is defined as the surface composed of end points of all the rays emitted from one light resource at the same instant of time. The shape of the ideal wavefront is a sphere, called the reference sphere, with center on the image plane. However, due to the thickness anomalies of the tear film, corneal distortion and other defects of the intraocular tissue, the aberrated wavefront arises. The wavefront aberration is then

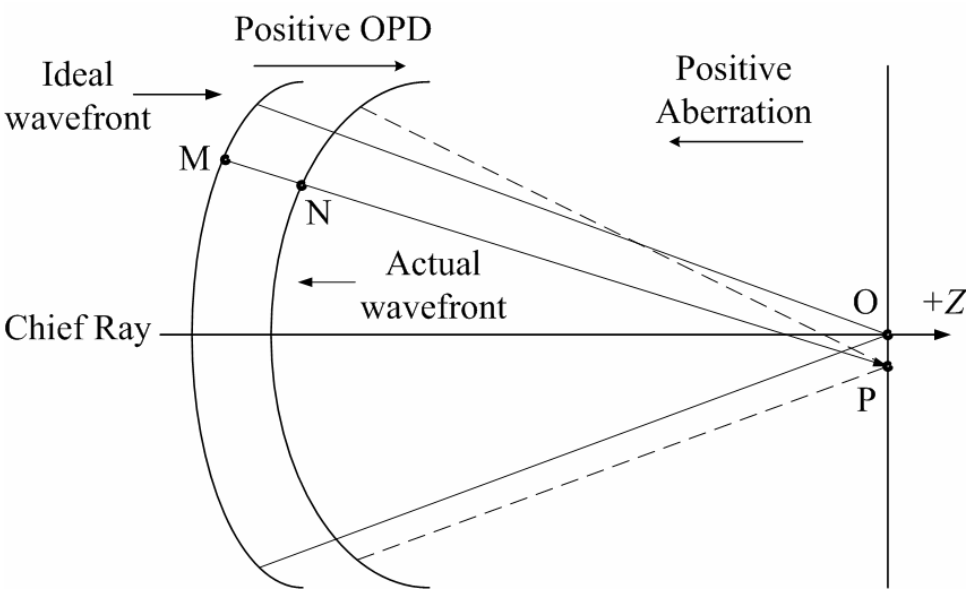

Figure 2.7 OPD for positive aberration.

defined as the optical path difference (*OPD*) between the ideal and actual (aberrated) wavefront (Wyant and Creath, 1992).

As shown in Figure 2.7, when a light ray passes the ideal wavefront at M and the actual wavefront at N, its wavefront error can be defined as the optical path difference (*OPD*) between M and N. That is

$$OPD = OPL_M - OPL_N \tag{2-4}$$

in which OPL_M is the *OPL* from the object to M and OPL_N is the *OPL* from the object to N. The *OPD* is positive if the aberrated wavefront leads the ideal wavefront as shown in Figure 2.7 (Wyant and Creath, 1992).

Hartmann-Shack wavefront sensor is widely applied in clinical ophthalmology to obtain the wavefront aberration map. The Hartmann-Shack method was used to eliminate the aberrations caused by turbulence in the earth's atmosphere to improve telescopes' use in astronomy. In 1994, Liang *et al*. found the possibility to use this approach to evaluate the eye and was the first to introduce it to ophthalmology (Liang *et al*., 1994). Since it offers advantages in terms of accuracy, reliability, rapidity and what is more important, there is a large amount of scientific literature and important

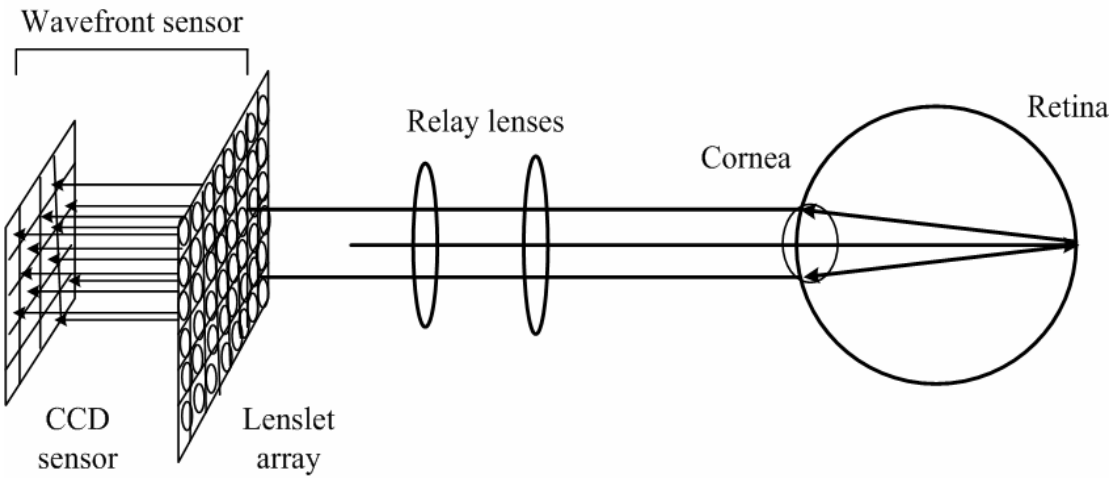

Figure 2.8 The modern aberrometer built on the Scheiner-Hartmann-Shack principle.

technological developments available for its application, the Hartmann-Shack wavefront sensor became the most popular measurement system to analyze aberration structure of human eye and a strong aid for corneal ablative pattern design (Lawless and Hodge, 2005).

Liang's concept of the Scheiner-Hartmann-Shack aberrometer is shown in Figure 2.8. It is important to analyze the reflected wavefront as soon as it leaves the exit pupil, because the shape of an aberrated wavefront surface changes as it propagates. A pair of relay lenses is used in this aberrometer model to focus the lenslet array onto the entrance pupil of the eye. Optically, the lenslet appears locating on the plane of entrance pupil to measure the reflected wavefront without any phase shift.

As shown in Figure 2.8, the reflected wavefront passes the micro lenslet array and finally focuses on a flat-plate CCD sensor. In a perfect eye, the reflected plane wave will be focused into errorless images with each point locating on the optical axis of the corresponding lenslet (displayed as Figure 2.9a). Otherwise, the aberrated wavefront shows a distorted grid pattern as shown in Figure. 2.9b.

It can be seen that the local slope of the wavefront is different for each lenslet, and therefore the wavefront will be focused into an irregular grid pattern. By measuring the displacement of each point from its corresponding lenslet axis, the slope of the aberrated wavefront when it entered the lenslet can be calculated. After mathematical integration of the slope, the final aberration map will also be obtained. A detailed

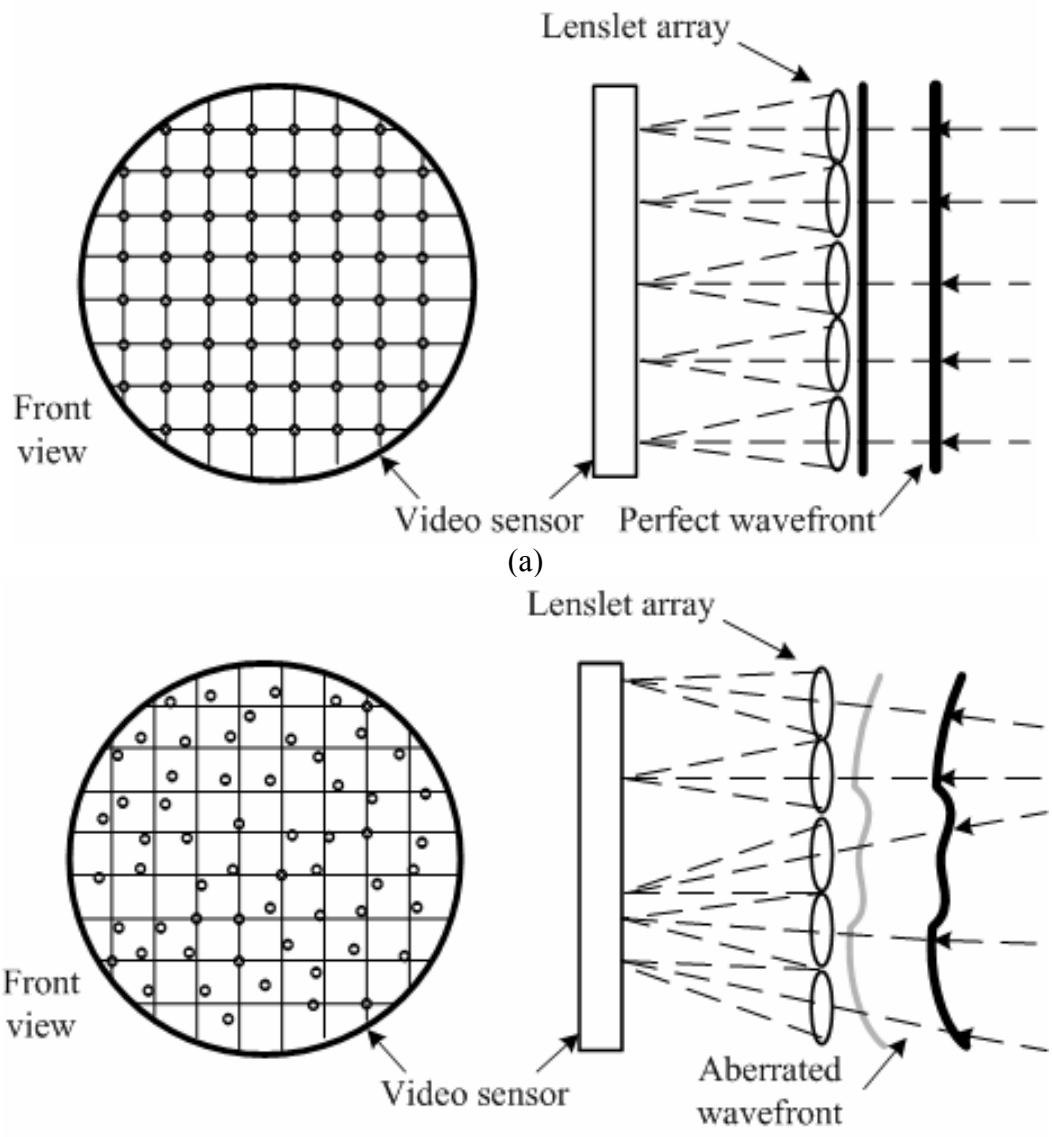

Figure 2.9 Grid pattern of (a) the ideal wavefront, and of (b) aberrated wavefront.

algorithm of calculating the aberration map from the wavefront slope is described by Liang *et al*. (1994).

2.1.4 Ray-trace technology

Another principle technology employed in ocular wavefront analysis is ray tracing. Tscherning introduced the ray tracing method to describe the eye's monochromatic aberrations first in 1894. It was adapted by Howland *et al.* in 1977 and then subsequently modified by Mierdel *et al.* in 1997 (Moreno and Navarro, 2000). In their

approach, a pre-determined pattern is projected onto the retina, and the aberration of the eye is calculated by using the amount of resulting shape distortion.

A modern laser ray tracing system projects a programmable laser that serially forms spots on the retina. After determining the spot positions, a ray-tracing algorithm is used to reconstruct the wavefront pattern of the whole eye. By changing the projected pattern, the spatial resolution can be increased, which is an advantage over the Hartmann-Shack method. However, a higher spatial density also increases the time needed for measurement.

In this report, a simplified ray trace process (Mahajan, 1998) carried on the anterior corneal surface is introduced to calculate the wavefront aberration of anterior corneal surface only, which is used in Chapter 5 to study the interplay of wavefront aberration of the cornea and intraocular components.

To calculate the wavefront aberration from the corneal data, firstly, the normal at each point on the corneal surface must be estimated. For 2-D ray tracing, the normal locates in the meridional plane and is specified by the angle it makes with the *z*-axis, indicated by ϕ in Figure 2.10. In a 3-D condition, the normal is specified by a vector n as shown in Figure 2.11.

After the normal is estimated, ray tracing can be conducted using Snell's law in either 2 or 3-D to calculate the optical path difference (*OPD*) directly.

Other methods calculating the corneal wavefront directly from the topographic data were also reported (Schwiegerling and Greivenkamp, 1997; Guirao and Artal, 2000), however, they came with different limitations.

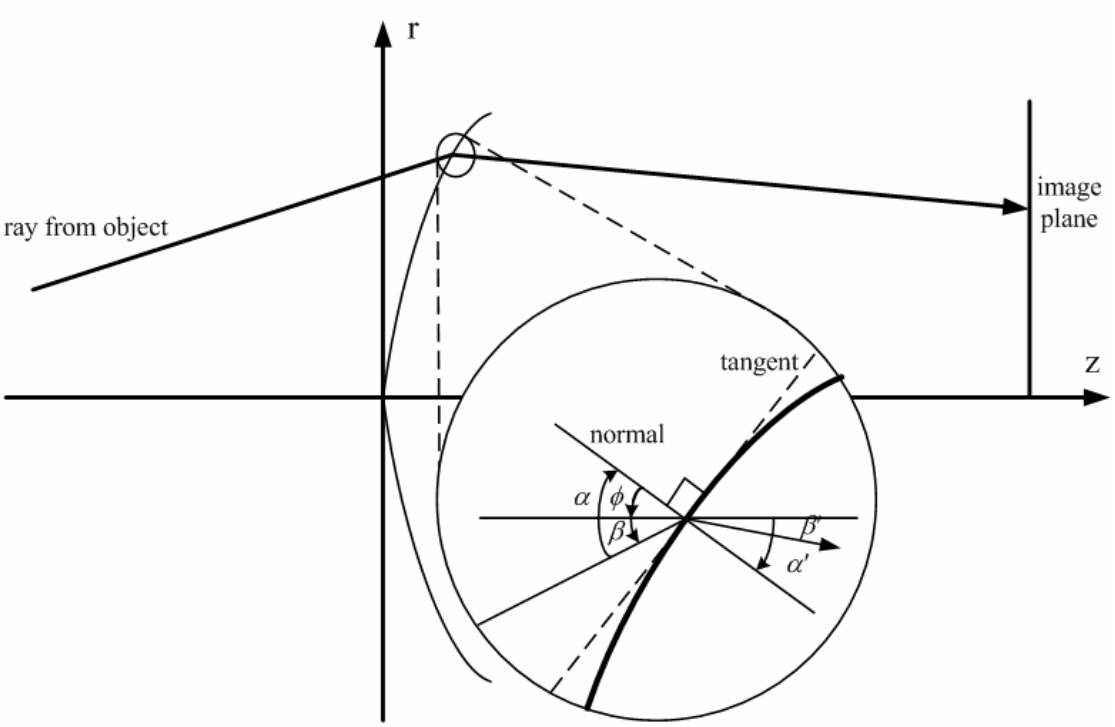

Figure 2.10 Ray tracing in 2-D.

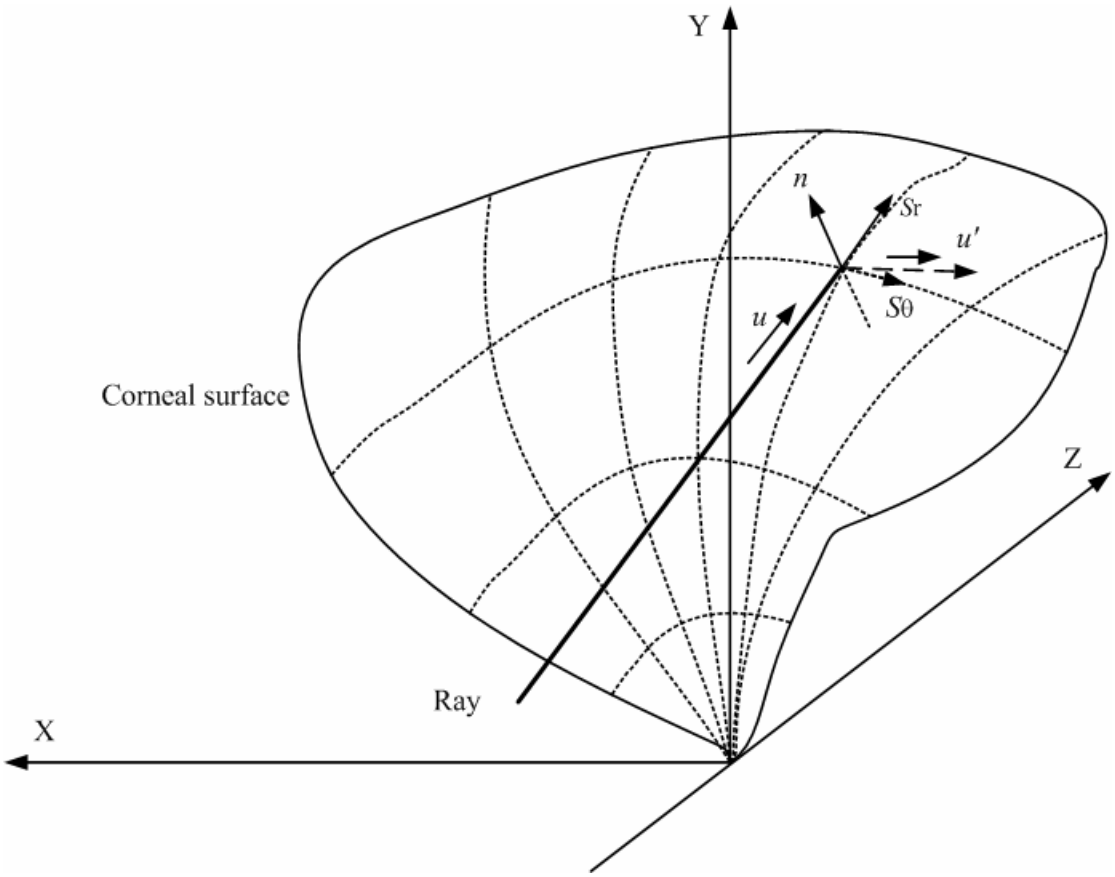

Figure 2.11 Ray tracing in 3-D.

2.1.5 Modeling wavefront data with Zernike polynomials

In this study, the topographic data of corneal surface is collected by a videokeratoscope (Keratron, Optikon), and the total aberration of eye is measured by a special Hartmann-Shack wavefront sensor (COAS, Wavefront Science, Inc.). A suitable mathematic tool is necessary to quantify and analyse these discrete data series, which is Zernike polynomials. The Zernike polynomials are a set of functions that are orthogonal over the unit circle (Iskander *et al.*, 2001). They are useful to describe the shape of an aberrated wavefront in the pupil of an optical system. The Zernike polynomials have been widely adopted as a standard for representing wavefront aberrations of the eye and corneal topographic aberrations in vision sciences. Because the Zernike series is orthonormal, a corneal surface with aberrations can be decomposed into different Zernike modes, analysed mode by mode to study the aberration distribution, and then recombined (Iskander *et al.*, 2001).

The wavefront aberration can be modeled by a finite series of Zernike polynomials

$$W(\rho,\theta) = \sum_{p=1}^{P} a_p Z_p(\rho,\theta) + \varepsilon(\rho,\theta) \qquad (2\text{-}5)$$

In the above equation:

$W(\rho,\theta)$ wavefront aberration;

index p polynomial-ordering number;

$Z_p(\rho,\theta)$ pth Zernike polynomial;

p =1, 2… P;

a_p coefficient associated with $Z_p(\rho,\theta)$;

p order;

ρ normalized distance from the origin;

θ angle;

$\varepsilon(\rho,\theta)$ measurement and modeling error (noise)

The pth-order Zernike polynomial is defined as

$$Z_p(\rho,\theta)=\begin{cases}\sqrt{2(n+1)}R_n^m(\rho)\cos(m\theta), & \text{even } p, m\neq 0\\ \sqrt{2(n+1)}R_n^m(\rho)\sin(m\theta), & \text{odd } p, m\neq 0\\ \sqrt{n+1}R_n^0(\rho), & m=0\end{cases} \tag{2-6}$$

where

$$R_n^m=\sum_{s=0}^{(n-m)/2}\frac{(-1)^s(n-s)!}{s!(\frac{n+m}{2}-s)!(\frac{n-m}{2}-s)!}\rho^{n-2s} \tag{2-7}$$

in which n is the radial degree and m is the azimuthal frequency.

The Zernike terms $Z_p(\rho,\theta)$ p =1,2…15, represent aberrations up to the 4th radial order including:

Lower-order aberrations:

Z_1 (piston); Z_2, Z_3 (tilts); Z_4 (defocus); Z_5, Z_6 (astigmatism);

Higher-order aberrations:

Z_7, Z_8 (comas); Z_9, Z_{10} (trefoils)

Z_{11} (spherical aberration), Z_{12}, Z_{13} (secondary astigmatisms)

Z_{14}, Z_{15} (tetrafoils)

2.2 Modern refractive surgeries

Different methods to improve the vision performance of eyes with refractive errors have been developed. Traditional corrections including the use of glasses and contact lenses to help correcting conventional aberrations by adding additional optical medium to affect the optical path, while laser vision correction provides a completely different correcting way by directly reshaping the cornea.

2.2.1 Principle of clinical laser vision correction

The application of laser in clinical refractive surgery is based on the knowledge of interaction between laser and the human eye tissue, especially the changes caused by laser irradiation involving mechanical, physical, chemical and biological aspects. The

structural and biological characteristics of human eye have made it the obvious beneficiary of laser refractive treatment.

i) Reflection and transmission of laser light in the human eye

The reflection of laser light in the human eye is one of the most important factors affecting the effectiveness of laser treatment. The refractive index of cornea is approximately 1.376. For normal incident laser beam, there is only a two-percent reflection rate on the anterior surface. Due to the smoothness of anterior corneal surface, energy loose of incident laser beam is mainly from mirror reflection, while diffuse reflection is negligible. Also, tear film in human eye, which acts as an anti-reflection layer, further reduces the reflection from corneal surface (Sun *et al*., 2002). To summarize, the human eye can be treated as an optical system with a negligible reflection rate for normal incident ray.

Incident light with a wavelength between 400~1400 *nm* is capable to travel through the refractive components in the human eye and reach the retina. After it passes the pupil (which has a diameter of approximately 5 *mm* under normal illumination) and focuses on the retina, a 5~50 μm diametric real image will be formed. Because the area of pupil is almost 10^5 times to the image size, the energy density on image spot will be 10^5 times larger than that on pupil, which means that after being focused, even a weak laser beam can cause serious damage to the retina.

ii) Absorptivity of ocular tissue to different wavelength of the laser beam

Study of absorption rate of laser energy in different ocular tissue provides the initial theoretical support for clinical laser corneal surgery. Absorption rates of refractive components to different wavelength of laser are shown in Table 2.1 (Sun *et al*., 2002).

It is found that for laser beam with a wavelength less than 280 *nm* or greater than 2000 *nm*, the cornea has almost a 100 percent absorption rate, which means using the laser beam within these two spectrum bands can efficiently avoid radiant damage to other eye tissue. In modern refractive surgery, 193 *nm* excimer laser is widely used.

Table 2.1 Absorption rates of ocular refractive components to different wavelength of a laser beam.

Wavelength (*nm*)	**Absorption Rate** (%)			
	Cornea	**Aqueous**	**Crystalline lens**	**Vitreous body**
280	100	0	0	0
300	92	6	2	0
320	45	16	38	1
340	37	14	48	1
360	34	12	52	2
360~400			Main receiver	
780~1400			Main receiver	
1400~1900	Main receiver	Main receiver		
>2000	100	0	0	0

iii) Clinical excimer laser and photoablation

The clinical application of excimer laser technology in ophthalmology was initiated in 1983 (Li and Zhu, 2001). In the research program held by Trokel and IBM researchers, it was discovered that the 193 *nm* ultraviolet light produced by ArF laser had a photoablation effect on the illuminated corneal tissue, which caused only micro thermal effect that could be ignored, but did significant stromal tissue ablation. Comparing to ablation done by infrared laser, much less thermal injury was observed under a microscope. The principal of physical process of photoablation is shown in Figure 2.12.

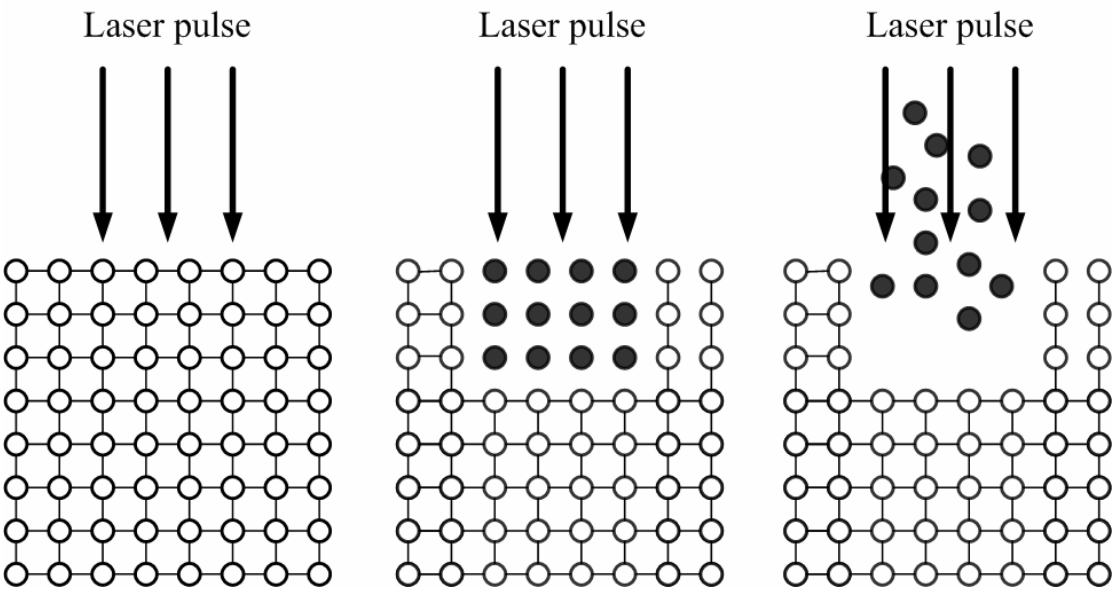

(a) UV laser illumination (b) Absorbtion of energy (c) Bound breaking

Fig 2.12 The stages of photoablation process

According to the photon energy formula (Equation 2-8), each photon in this case carries 6.4 electron-volts energy (Yang, 2000), while the chemical bond of carbon chains in the corneal tissue molecule is only 3.4 electron-volts (Li and Zhu 2001). Because the corneal stromal tissue has an almost full absorption rate for this type of photon energy, when high-power 193 *nm* excimer laser is illuminating on the corneal surface, bond breaking occurs in the tissue molecules. After absorption of the laser energy, this part of tissue is then completely evaporated to a dissociated state.

$$\varepsilon = \frac{h \cdot C}{\lambda} \tag{2-8}$$

In the above equation, h=6.626$\times 10^{-34}$ *J.S* stands for the Planck constant, C represents the velocity of light and λ is the wavelength of the laser beam.

By means of setting the illumination mode and target area on the corneal surface and delivering the pre-calculated number of pulses, the pre-determined amount of stromal layer is removed by photoablation to change the partial corneal thickness and curvature. The excimer laser apparatus delivers continuous pulses to the corneal

surface during the surgical process. Each pulse removes only 0.25 micron of tissue while the total corneal thickness is approximately 550 μm, which guarantees the ablating precision (Krueger and Trokel, 1985; Kurtz *et al.*, 1997).

2.2.2 LASIK procedures

In this section, treatments of defocus and astigmatism are taken to explain the LASIK surgical process performed by a broad beam laser.

After measuring the total wavefront aberration and elevation data of corneal surface, a target surface of ablation is calculated by the computer system, and the following procedures are delivered:

i) Creating a flap on the corneal surface

Firstly, using a special microkeratome instrument, an extremely thin flap (approximated 80~120 microns) on the corneal surface is created. When cutting action completes, the flap is left connected to the corneal surface. Then the corneal flap is folded back to expose the inner layer called stromal bed, on which the refractive incision will be performed.

ii) Excimer laser treating on the exposed corneal stroma

According to different types of corneal aberrations, there are various methods of laser beam delivery. For myopia, the laser beam widens to reduce the curvature of cornea. The illumination period on middle part of the cornea is longer than the outer-ring, which means that more tissue is removed from the middle part than the out-ring area. After the treatment, the corneal surface is flatter. In the condition of hyperopia, the delivered laser beam expends as a shape of ring to steepen the central part of cornea. While treating the astigmatism, laser beam shape illuminating on the stromal layer is an oval fashion, which ablates the corneal surface more in one axis than the others. Generally, the maximum ablation depth has a linear relation to the amount of spherical aberration. The maximum depth of the ablation is also restricted by the patient's corneal thickness. A minimum residual thickness of 250 μm is required to

prevent the corneal shape change due to intra ocular pressure. However, 270~275 μm thickness of residual corneal tissue is recommended, which guarantees the safety of surgery and provides the margin for future enhancement (in some cases, second ablation is needed). Considering the thickness of flap and residual tissue, the maximum ablation depth allowed will be approximately 160~220 μm.

iii) Replacement of lamellar flap onto treated bed and the final result

After the treatment, the lamellar flap is replaced to the treated surface and self-adheres. LASIK has a significant effect in eliminating myopia from –1.00 to –9.00 diopters, and provides a good general benchmark in treating hyperopia within the range from +1.00 to +6.00 diopters. Obvious visual enhancement is also observed on patients with mild or middle degree astigmatism after LASIK treatment (MacRae *et al.*, 2000; McGhee *et al*., 2001). However, studies based on aberrations and visual performance demonstrate that the best-corrected image quality degrades after the LASIK treatment (Mrochen *et al.*, 2001; Scisco *et al*., 2003; Shimmick *et al*., 1997) which is often due to the increased higher-order aberrations (HOA). Reasons of the observed increase of HOA include:

1) Methods for calculating ablation profiles

Several methods of generating ablation pattern for corneal correction have been proposed and their efficiency theoretically examined. They focus on elimination of different types of aberrations and require different instruments to collect corresponding parameters. Manns *et al.* (2002) presented a method to calculate ablation profiles for correction of both defocus and primary spherical aberration. The method requires not only the refractive error and wavefront sensor data, but also the preoperative corneal radius and asphericity factor as well as the internal eye aberrations. Jimenez *et al.* (2001) defined the ablation profile by using radius of curvature and corneal asphericity in different meridians and the amount of induced corneal spherical aberration was used to adjust the ablation pattern. Klein (1998) developed an algorithm in which corneal shape information is omitted and only the total wavefront aberration is utilized. The surgical result varies due to adoption of different method to calculate ablation profile.

2) Scanning algorithms and spot size.

Due to the natural curvature of the corneal surface, the incident angle of laser beam changes when moving from the corneal apex to periphery, which leads to the change of ablation depth for each pulse resulting undercorrction in periphery (Mrochen and Seiler, 2001; Anera *et al.*, 2003; Jimenez *et al.*, 2004). Precise mathematical algorithms are desired in cases with scanning laser to determine the overlapping of laser spots, which can greatly affect the postoperative corneal smoothness (Manns *et al.*, 1995; Homolka *et al.*, 1999). The studies of influence of spot size in refractive surgery also indicate that the use of spots larger than 0.5 *mm* might not be effective to completely correct vision error, and some HOA could be induced after the ablation (Fiore *et al.*, 2001; Huang, 2002; Guirao *et al*., 2003).

3) Decentration

Very small displacement of the treatment zone with respect to the line-of-sight (LOS) can induce large amount of HOA degrading the vision performance after surgery (Guirao *et al.*, 2000; Alessio *et al.*, 2001; Donnenfeld, 2004; Mrochen *et al.*, 2002). It is also a major factor affecting the outcomes of theoretical studies of corneal ablation. Modern eye tracking systems are developed to overcome the problem (Mrochen *et al*., 2001; Bueeler and Mrochen, 2004).

4) Other factors

Other factors increasing the HOA include flap-induced aberration, self-recovery of corneal tissue and biomechanical changes (Chuck *et al*., 2001; Pallikaris *et al.*, 2002). The influence of the first three aspects will be discussed in detail in the following chapters and feasible solutions will be proposed. They are also the focus points in the author's MPhil study.

Chapter 3

Ablation Profile Calculation

Algorithms calculating the ablation profiles for laser refractive surgery improve with the development of clinical laser technologies. The early methods mainly focused on eliminating defocus and astigmatism. After the introduction of modern wavefront sensing and scanning laser techniques, comprehensive vision error correction is becoming possible, leading to the development of wavefront optimised corneal ablation. Therefore, algorithms calculating high-precision ablation profiles from the wavefront aberration maps have been developed.

The design of ablation profiles is usually based on theoretical eye models, which represent the optical behaviour of the average human eye. Munnerlyn *et al*. (1988) proposed one of the early methods using the refractive power and shape of the anterior corneal surface to calculate the amount of tissue removal for spherocylindrical correction within a given optical zone.

3.1 Approximated Munnerlyn formula

Approximated Munnerlyn formula is widely used to determine ablation profile for correcting defocus (Chang *et al*., 2003). It is theoretically based on the assumption that both the cornea and ablation profile are spherical (Munnerlyn *et al.*, 1988).

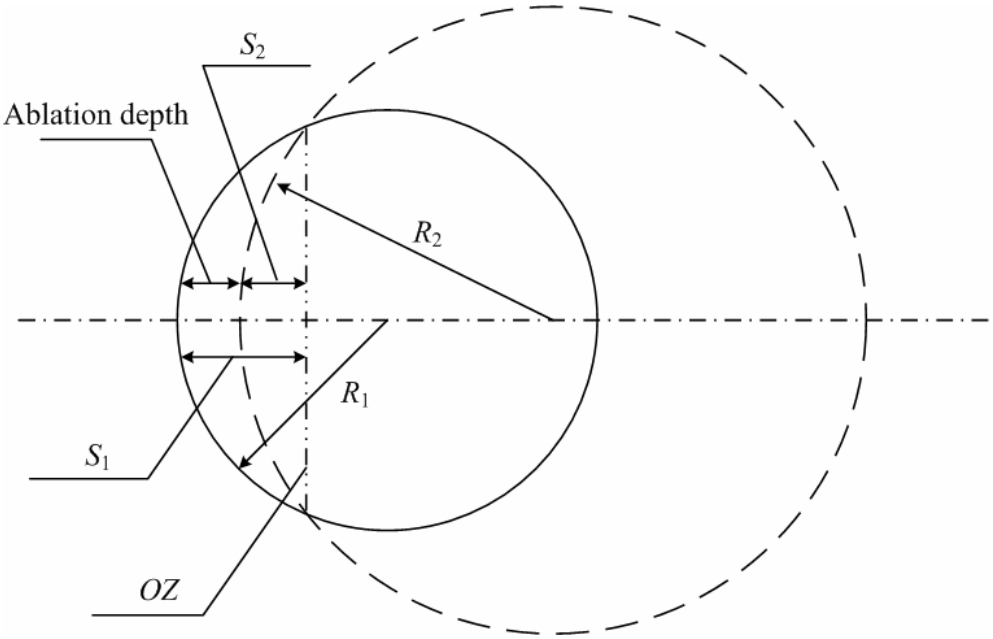

Figure 3.1 Ablation depth for spherical Myopia.

In myopic eyes, the ablation depth is generated along the optical axis as shown in Figure 3.1. The exact ablation depth for spherical geometry is calculated by

$$D_{th} = R_1 - \frac{R_1 \times (n-1)}{n-1+R_1 \times D_1} - \sqrt{R_1^2 - \frac{OZ^2}{4}} + \sqrt{\left[\frac{R_1 \times (n-1)}{n-1+R_1 \times D_1}\right]^2 - \frac{OZ^2}{4}} \qquad (3\text{-}1)$$

where n is the refractive index of the cornea, D_1 is the amount of correction in diopters , R_1 and R_2 represent initial and final radius of curvature respectively; OZ is the diameter of the ablation zone, while S_1 and S_2 indicate the sagittal depth of the preoperative and postoperative cornea respectively.

In Figure 3.1, the ablation depth at the optical axis is illustrated as the difference between the sagittal depth of the preoperative and postoperative cornea. In general, for any circle of radius R, the exact sagittal depth is

$$S = R - \sqrt{R^2 - \frac{OZ^2}{4}} = R\left(1 - \sqrt{1 - \frac{OZ^2}{4R^2}}\right) \qquad (3\text{-}2)$$

The square root term can be expressed in a power series

$$\sqrt{1-\left(\frac{OZ}{2R}\right)^2} \cong 1-\frac{OZ^2}{8\times R^2}-\frac{OZ^4}{128\times R^4}-\frac{OZ^6}{1024\times R^6}-HOT \tag{3-3}$$

where *HOT* stands for the higher order terms. Because the diameter of ablation zone is smaller compared to the central radius of the corneal curvature, only the first two terms are considered. The approximated sagittal depth becomes

$$S_A \cong R\left[1-\left(1-\frac{OZ^2}{8R^2}\right)\right]=R\left(\frac{OZ^2}{8R^2}\right)=\frac{OZ^2}{8R} \tag{3-4}$$

Therefore, the approximated ablation depth becomes

$$D_A=\frac{OZ^2}{8}\left(\frac{1}{R_1}-\frac{1}{R_2}\right) \tag{3-5}$$

Because the paraxial power of the anterior corneal surface is

$$P=\frac{(n_c-1)}{R} \tag{3-6}$$

where n_c is the refractive index of the cornea, the amount of correction in dioptors becomes

$$D_1=P_f-P_i=(n_c-1)\left(\frac{1}{R_2}-\frac{1}{R_1}\right) \tag{3-7}$$

P_f and P_i indicate the final and initial paraxial power of the anterior corneal surface respectively. Thus,

$$\left(\frac{1}{R_2}-\frac{1}{R_1}\right)=\frac{D_1}{(n_c-1)} \tag{3-8}$$

the Equation (3-5) becomes

$$D_A = -\frac{OZ^2}{8}\left(\frac{D_1}{n_c - 1}\right) \tag{3-9}$$

The value of n_c is taken by Munnerlyn as 1.377, then the approximated Munnerlyn formula for clinical use becomes approximated by

$$D_A \cong \frac{OZ^2}{3} D_1 \tag{3-10}$$

The calculation of ablation depth with Munnerlyn formula is only based on topographic information, which limits its predictability of visual improvement and application for higher order aberrations (HOA) correction.

After Munnerlyn's method, more topography-based approaches have been attempted with limited success (Seitz *et al.*, 1998; Wiesinger *et al.*, 1998; Dausch *et al.*, 2000; Knorz and Jendrita, 2000). Refractive analysis with higher precision in a small corneal area is adopted by topography-guided technologies, such as TOPOLINK (Alio *et al.*, 2003) and C-CAP method (Brown and Campbell, 2003), to achieve some correction of HOA. However, the results of these technologies have been inconsistent and secondary visual defects are induced in some cases.

3.2 Ablation profiles for wavefront optimized corneal correction

As mentioned earlier, a recent development of laser refractive surgery is wavefront optimized corneal ablation, which combines the advantages of small spot scanning laser and modern wavefront sensing technology. It has the potential to not only eliminate defocus and astigmatism but also reduce the higher order aberrations, which makes it a feasible solution for cases with complicated vision error or after previous unsuccessful refractive surgery (Gibralter and Trokel, 1994; MacRae *et al.*, 2000; Huang, 2002; Mrochen *et al.*, 2004 a).

Several algorithms for calculating ablation profiles of wavefront optimal refractive correction were proposed and their efficiency theoretically examined.

3.2.1 Klein's wavefront only approximation

Klein (1998) presented an algorithm for calculating the optimal amount of ablation with only the knowledge of HS wavefront data, and suggests that the aberrations alone are sufficient to accurately specify the corneal ablation, while shape of cornea is less relevant.

With an original purpose of combining both wavefront and topographic data to specify a new corneal shape with ideal optics, HS data and corneal elevations are used in Klein's method.

The calculation starts from the HS data, which specify the location (x_{HS}, y_{HS}, z_{HS}) of a given HS lenslet and direction ($\hat{V}_{HS}$) of the ray emerging from the cornea. A coordinate system has the corneal vertex as the origin, with the corneal normal at the vertex pointing onto the eye, in the +z direction, is adopted as shown in Figure 3.2.

After the rays are refracted by the cornea, the direction becomes $\hat{V}$, as indicated in Figure 3.2. The blown up detail of one of the lenslets shows two adjacent rays hit the HS plane in points *a* and *b*.

Based on the given slope of each ray from the HS data, a backwards ray tracing can be done because the reversibility of optical path to find out the shape of the wavefront, which is necessary for calculating the optimal corneal shape.

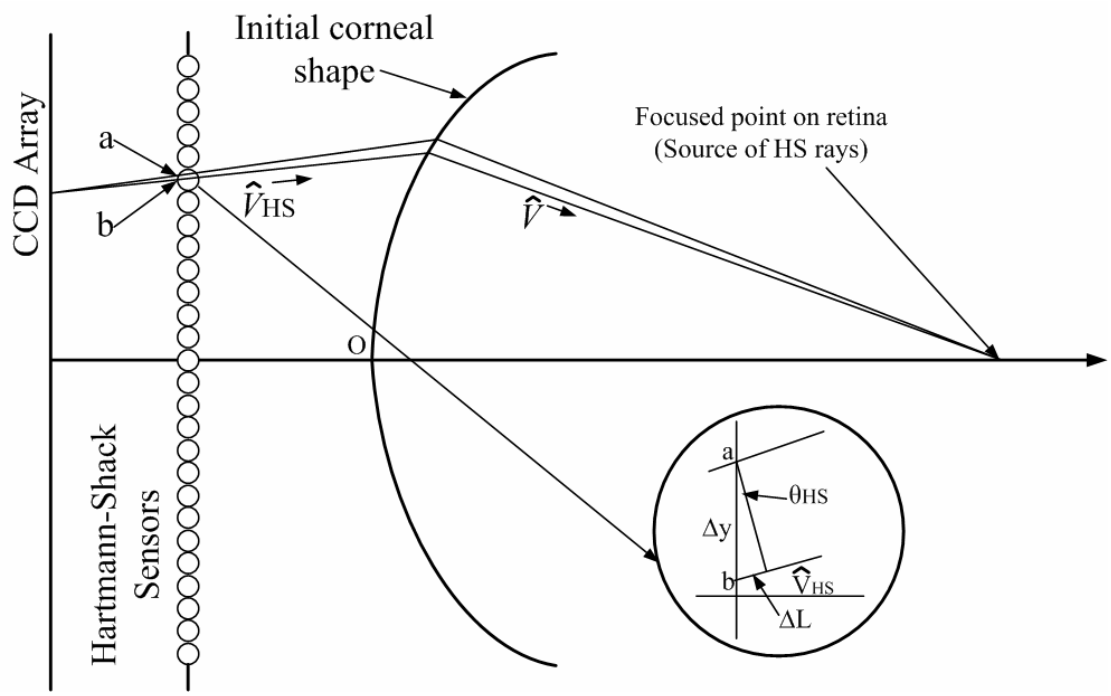

Figure 3.2 HS sensors measuring aberrations from the eye.

Klein also provides a second method to obtain the target corneal shape by generating the wavefront phase at the HS sensors and then calculating the amount of ablation that produces this wavefront from incoming plane waves. The final achieved ablation depth is given by

$$D_{c-A} = [E + z_c - L - (z_c + d)/V_{HS,z}]/(n - V_z) \tag{3-11}$$

where L is the initial optical path length obtained from the wavefront phase, d is the distance from HS plane to the corneal vertex. E indicates the location of reference plane, which controls the ablation depth. The z component of the considered unit vector can be calculated from $V_{HS,z} = \cos(\theta_{HS})$. For a myopic eye, E is given by:

$$E = -\max[z_c - L - (z_c + d)/V_{HS,z}] \tag{3-12}$$

to generate maximum central ablation depth and minimum value at periphery as shown in Figure 3.3.

On the other hand, E for a hyperopic case is given by

$$E = -\min[z_c - L - (z_c + d)/V_{HS,z}] \tag{3-13}$$

to limit the ablation depth $D_{c\text{-}A,}$ which never goes negative and a minimum depth of zero is obtained in the ablation center as displayed in Figure 3.4.

To prove the minimum effect of corneal shape in specifying the ablation profile, Equation (3-11) is then simplified by removing quantities z_c and V_z that depend on corneal shape. The approximated equation becomes:

$$D(x,y) = [E - d/V_{HS,z} - L(x,y)]/(n-1) \tag{3-14}$$

For correction of hyperopia, *E is* determined by Equation (3-13). Equation (3-14) is rewritten as

$$D(x,y) = \{d[\max(1/V_{HS-z}) - 1/V_{HS-z}] + \max(L) - L(x,y)\}/(n-1) \tag{3-15}$$

which is further approximated to

$$D(x,y) = d\theta^2/(2(n-1) + [\max(L) - L(x,y)]/(n-1) \tag{3-16}$$

in which the distance from HS plane to corneal vertex is taken to be d (minus 3 *mm*), based on Liang and Williams's design (Liang *et al.*, 1994), which places the HS to the entrance pupil by introducing relay lens. θ depends on the amount of incoming vergence and pupil size. For example, a 5-diopters incoming vergence will give an angle of $\theta = 0.003 \times 5 = 0.015$ *rad* at a radius of 3 *mm* from the axis. And an assumption is made to let optical path length $L(x,y)$ be equal to the wavefront, $W(x,y)$. Therfore, the above formula becomes

$$D(x,y) = d\theta^2/(2(n-1) + [\max(W) - W(x,y)]/(n-1) \tag{3-17}$$

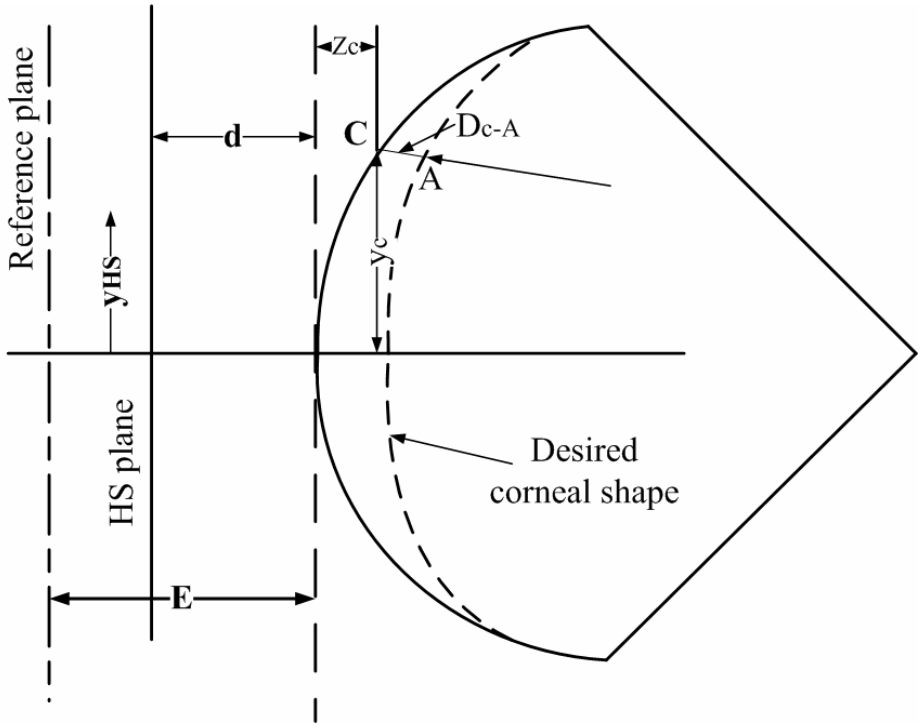

Figure 3.3 Ablation pattern for myopia.

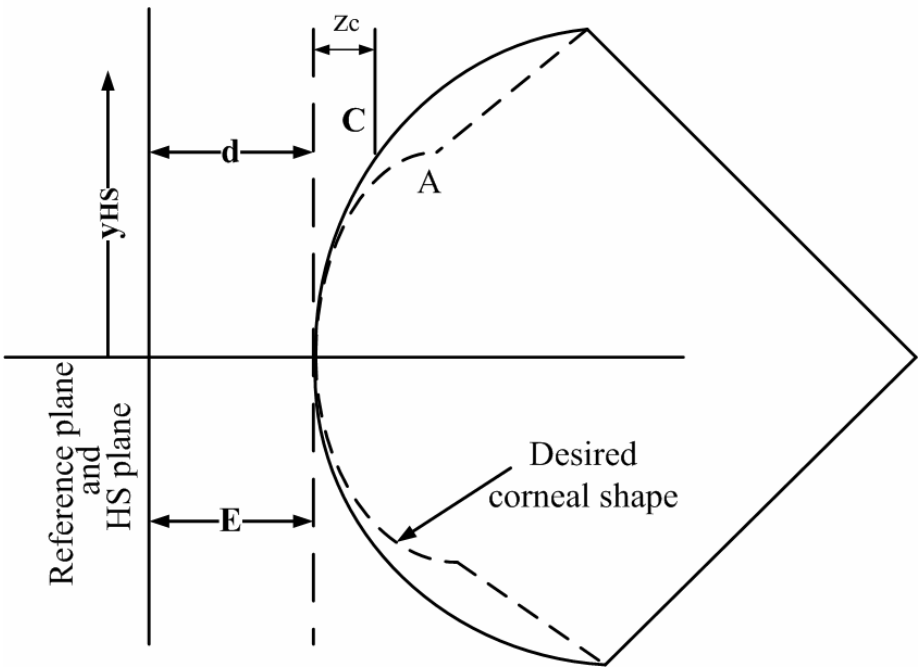

Figure 3.4 Ablation pattern for hyperopia.

3.2.2 Mrochen *et al.*'s wavefront optimized ablation method

Mrochen *et al*. (2004) summarized the procedures to calculate an ablation profile for general wavefront-optimized surgery in three general steps:

i) Measure and map the total aberrations

Accurately measuring and mapping wavefront aberrations from the human eyes has been realized after the introduction of Hartmann-Shack wavefront sensing technology by Liang *et al.* (1994). A high precision wavefront map represents the optical defects caused by different aberrations and provides the basis of aberration analysis and wavefront-guided ablation pattern calculation.

ii) Inverse the wavefront map

The aim of wavefront-guided ablation is to correct the wavefront, the wavefront map need to be inversed.

iii) Converse the wavefront to ablation depth

In refractive surgery procedures, the correction of wavefront is achieved by ablating the cornea. Because the ablation only removes tissue rather than adding tissue, the wavefront correction must be considered by shifting the ablation map to only positive value. Furthermore, the ablation is performed by modifying the anterior corneal surface, the refractive index change from air (n_1=1) to the tear film boundary (n_2=1,337) must also be included. The conditions above are implemented in a formula for the desired ablation depth for an arbitrary point (ρ,θ) that is given by (Mrochen *et al.*, 2004 b)

$$a(\rho,\theta) = \frac{|W(\rho,\theta)|_{\max} - W(\rho,\theta)}{n_2 - n_1} \tag{3-18}$$

where $|W(\rho,\theta)|_{\max}$ represents the maximum wavefront out of all rays as displayed in Figure 3.5(c).

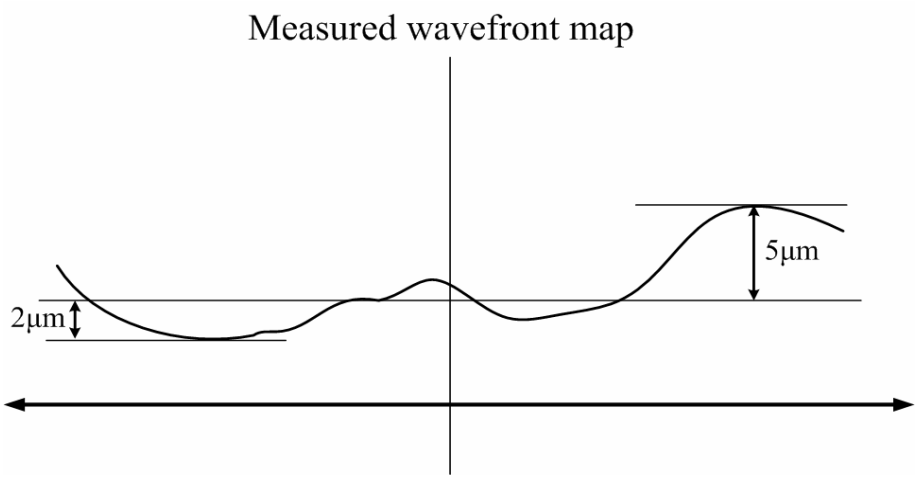

(a)

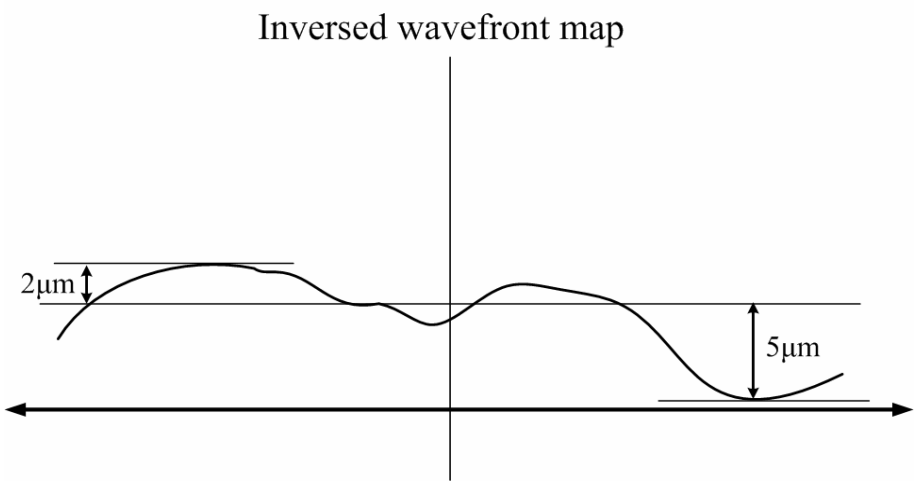

(b)

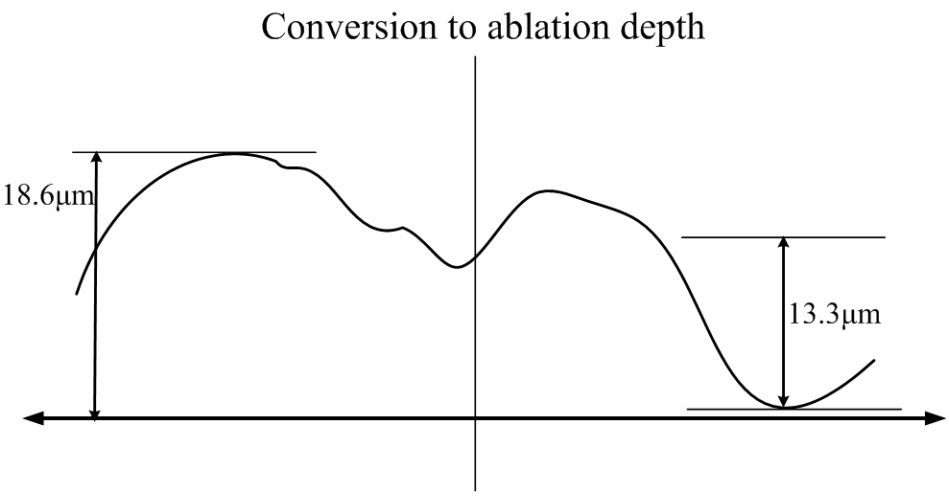

(c)

Figure 3.5 The three steps in Mrochen *et al*. formula (a) Measure and map total wavefront. (b) Inverse the wavefront map. (c) Converse wavefront to ablation depth.

When wavefront errors are described by a series of Zernike polynomials, the wavefront optimized ablation profile of different aberrations can be decomposed into individual terms (Iskander *et al.*, 2001). For example, the ablation profile of a spherocylindrical correction based on the second order Zernike polynomials reads

$$a(\rho,\theta) = \frac{|W(\rho,\theta)|_{\max} - W(\rho,\theta)}{n_2 - n_1}$$

$$= \frac{2Z_2^0(1-\rho^2) + \sqrt{\left(Z_2^{-2}\right)^2 + \left(Z_2^2\right)^2} - Z_2^{-2}\rho^2\sin(2\theta) - Z_2^2\rho^2\cos(2\theta)}{n_2 - n_1} \qquad (3\text{-}19)$$

while spherocylindrical wavefront aberrations are described by

$$W(\rho,\theta) = Z_2^0(2\rho^2 - 1) + Z_2^{-2}\rho^2\sin(2\theta) + Z_2^2\rho^2\cos(2\theta) \qquad (3\text{-}20)$$

This is the polar representation with the relative pupil size $\rho = r/R$ raging from 0 to 1; r is the radius ranging from 0 to R, and the angle θ is measured anticlockwise from the positive x axis.

3.2.3 Manns *et al.*'s algorithm

A method calculating the ablation profiles for wavefront-guided correction of ametropia and primary spherical aberration is proposed by Manns *et al*. (2002). It is found that the contribution of each ocular surface to the primary spherical aberration can be expressed in terms of the ray height at the anterior corneal surface. The method is applied to calculate the ablation profile in Manns *et al.*'s study.

A modified Navarro model (Navarro *et al.*, 1985) of the relaxed eye is used to simulate the human eye with axial myopia, which uses 4 aspheric surfaces to represent the cornea and lens as shown in Table 3.1:

Table 3.1 Parameters of the Navarro model of the relaxed eye.

Surface	Radius of curvature (mm)	Asphericity factor (Q)	Position (mm)	Refractive index of the incidence medium
Anterior cornea	7.72	– 0.26	0.00	1
Posterior cornea	6.50	0.00	0.55	1.367
Anterior lens	10.20	– 3.1316	3.55	1.3374
Posterior lens	– 6.00	– 1	7.55	1.42
Retina	∞	0	23.95	1.336

Correction of defocus is performed by changing the anterior corneal radius of curvature according to the approximated Munnerlyn formula. For a 6 *mm* ablation zone, with parameters of Navarro eye model, the postoperative corneal radius is given by

$$R_f = \frac{0.367}{47.5 - D_1} \tag{3-21}$$

in which D_1 is the desired amount of correction in Diopters (for myopia, $D_1>0$).

Correction of primary spherical aberration starts from calculating the contribution of each ocular surface to the spherical aberration of the postoperative eye. The value of postoperative anterior corneal surface asphericity factor, which is required to balance the sum of the contribution of the posterior corneal surface, anterior and posterior lens surface, Q_f is calculated. One assumption is made to simplify the calculation that the thickness of cornea is unchanged after ablation. With the numerical values of Navarro eye model, the contribution of anterior corneal surface to the spherical aberration is given by

$$W_1 = -\frac{0.046}{R_f^3} \times (0.535 + Q_f) \tag{3-22}$$

the value of the asphericity factor that minimizes the primary spherical aberration in the relaxed eye can be expressed as

$$Q_f = R_f^3 \frac{W_2 + W_3 + W_4}{0.046} - 0.535 \tag{3-23}$$

where W_2, W_3 and W_4 are the aberration coefficients of the posterior corneal surface, anterior lens surface and posterior lens surface, respectively.

By assuming the preoperative corneal surface as a conicoid with apex radius R_i and asphericity Q_i and using the formula for the height of a conic section, the expression of ablation profile, which produce a postoperative cornea with a radius of R_f and asphericity Q_f is obtained

$$\begin{aligned} a(r) &= Z_i(r) - Z_f(r) \\ &= -\frac{r^2}{R_i + \sqrt{R_i^2 - (1+Q_i)r^2}} + \frac{r^2}{R_f + \sqrt{R_f^2 - (1+Q_f)r^2}} + a(0) \end{aligned} \tag{3-24}$$

where r is the radial position and $a(0)$ is the central ablation depth. By setting the ablation depth at the periphery to zero, the Equation (3-23) changes to

$$a(r) = \frac{\frac{OZ^2}{4} - r^2}{\sqrt{R_i^2 - (1+Q_i)r^2} + \sqrt{R_i^2 - (1-Q_i)\frac{d^2}{4}}} - \frac{\frac{OZ^2}{4} - r^2}{\sqrt{R_f^2 - (1+Q_f)r^2} + \sqrt{R_f^2 - (1-Q_f)\frac{d^2}{4}}}$$

in which OZ is the diameter of ablation zone.

3.3 Future development of algorithms calculating ablation profiles

The concept of customized corneal treatment was proposed to improve eyes with poor optical quality due to corneal abnormalities. The first individualized corneal treatment was performed based on corneal topographic data, and showed the potential benefit of

the technology (Terry, 2000). However, the predictability of the procedures was unstable. Moreover, the induced HOA also limited the vision outcome of the early procedures (Gibralter and Trokel, 1994; Seitz *et al*., 1998; Fernandez and Serrano, 2000; Alio *et al*., 2003; Anderson *et al*., 2004).

The current wavefront-guided correction can provide subjectively and objectively better vision outcomes, and has the potential to improve HOA. Nevertheless, there are still limitations reducing the precision of the procedures, which include the repeatability and accuracy of the wavefront sensor and latency of eye tracking system (Guirao *et al*., 2000; Bueeler and Mrochen, 2004; Donnenfeld, 2004; Thibos *et al*., 2004).

A possible solution is combining wavefront and topography data together to design the ablation profile of customized ablation, which takes more factors into account to improve the predictability of the final result (Kohnen, 2004).

Chapter 4

A Comparison of Ablation Profile Methods

Choosing the right algorithm to calculate the ablation profile is one of the most important procedures in pre-surgical preparation for modern customized corneal correction.

In this chapter, a detailed comparison is performed among the ablation profile methods reviewed in Chapter 3 to select the most suitable algorithms for a comprehensive vision improvement. The algorithm will be examined using a computer simulation in Chapter 5. The following criteria were used for the comparison: (1) ability of correction of lower order aberrations (LOA) and higher order aberrations (HOA); (2) number of required parameters and (3) laser system requirements.

An extensive literature review on algorithms calculating the ablation pattern has been done during the author's MPhil study. Several major methods of generating the ablation pattern for corneal correction have been reviewed (Munnerlyn *et al*., 1988; Klein, 1998; Jimenez *et al.* (2001); Manns *et al*., 2002; Mrochen *et al*., 2004.).

Manns *et al*., (2002) presented a method to calculate ablation profiles for correction of both defocus and primary spherical aberration. The method requires not only the refractive error and wavefront sensor data, but also the preoperative corneal radius of

curvature and asphericity factor as well as the derived internal eye aberrations. For the latter they used a modified eye model of Navarro (1985). Jimenez *et al.* (2001) defined the ablation profile by using radius of curvature and corneal asphericity in different meridians and the amount of induced corneal spherical aberration was used to adjust the ablation pattern. This method requires knowledge of material properties, which was outside the scope of this research study. Klein (1998) developed an algorithm in which corneal shape information is omitted and only the total wavefront aberrations are utilized. Mrochen *et al*. (2004) further improved the method in their later work. Other methods based on the approximated Munnerlyn formula (Gatinel *et al*., 2002; Chang *et al*., 2003), use the refractive power and shape of the anterior corneal surface as main parameters and require a number of other factors such as corneal asphericity to calculate the amount of removed tissue.

Approximated Munnerlyn formula

Except those for customized corneal ablation, most ablation algorithms are still based on the paraxial formula by Munnerlyn *et al* (1988), which is now widely accepted by clinicians and also considered as a mature method to calculate the ablation depth for spherical correction (defocus). As reviewed in Chapter 3, the ablation depth for myopia by exact Munnerlyn formula is expressed as

$$D_{th} = R_1 - \frac{R_1(n-1)}{n-1+R_1D_1} - \sqrt{R_1^2 - \frac{OZ^2}{4}} + \sqrt{\left[\frac{R_1(n-1)}{n-1+R_1D_1}\right]^2 - \frac{OZ^2}{4}}$$

while the approximated ablation depth is given by

$$D_A \cong \frac{OZ^2}{3} D_1$$

which is derived from the first two terms of a Taylor series expansion as shown in Equation (3-3) and (3-4) in Chapter 3.

As a standard ablation profile method, which is still used by many clinicians nowadays, Munnerlyn formula has certain advantages. First of all, the approximated Munnerlyn formula is in quite a simple form. It can be seen from Equation (3-10) that the ablation depth predicted by approximated Munnerlyn formula only depends on two parameters: the size of optical zone and the amount of correction in diopters. The amount of correction in diopters can be easily obtained from a modern keratoscope and the size of optical zone is determined by the clinician. Secondly, clinical application of more than 10 years has shown that Munnerlyn's approximated formula is extremely accurate in small optical zone, of less than 5 *mm* in diameter (Munnerlyn *et al.*, 1988; Chang et al., 2003), especially for patients with a small amount of astigmatism and HOA. Furthermore, because of its simple ablation pattern, the requirement of surgical laser is relatively lower. For example, a 2 *mm* laser beam can produce an effective correction for ablation profile generated by the approximated Munnerlyn formula (Guirao *et al*., 2003). At the same time, the laser delivery algorithm is also simplified due to the large laser beam used. The basic LASIK procedures introduced in Chapter 2 without consideration of accurate spot overlap can be delivered in cases using the approximated Munnerlyn formula.

However, as an early profile method developed almost 20 years ago, the approximated Munnerlyn formula lacks of connection with modern visual-optical technologies and its application also comes with limits. The Munnerlyn's model is based on spherical geometry, which limits its application in correction of only defocus. As a result, aberrations such as astigmatism and HOA are not taken into account. Patients with a relatively higher amount of astigmatism and HOA will not have ideal surgical outcomes.

Because of the nature of approximation used, the ablation depth is always underestimated. At the time the Munnerlyn's method was derived, it was designed for an optical zone of 3~4 *mm* (Munnerlyn *et al*., 1988), in which the approximated formula is extremely accurate. However, for today's optical surgery with larger optical zone and correction, underestimation of ablation depth by using the approximated Munnerlyn formula becomes obvious, which brings risk for postoperative ectasia. For an average cornea, the difference of ablation depth between the exact and approximated Munnerlyn formula is 6.0 μm for a –5 diopters correction

in a 6 *mm* optical zone. The error is almost 10% comparing to the maximum ablation depth of 60 μm. For larger optical zones and correction, the results could be even worse.

Manns's Method for Myopia and Primary Spherical Aberration

Manns *et al*., (2002) presented a method of calculation of ablation profiles for the correction of defocus and primary spherical aberration, which was based on the Navarro model of the relaxed eye. Although Manns's method assumes that the cornea is a rotationally symmetric aspheric surface centered on the optical axis, which limits its ability to additionally correct cylinder, coma and other HOA, it combines the contribution of each corneal surface to primary spherical aberration and points out the possibility of applying this technology to correct other aberrations.

In Manns's method, the part of correction of defocus is based on the approximated Munnerlyn formula. For this reason, it comes with the same advantages and limitations for defocus correction as the approximated Munnerlyn method. However, to achieve complete removal of primary spherical aberration, the algorithm requires more input data. The parameters of the ablation algorithm include the refractive error, the preoperative corneal radius of curvature and asphericity factors (R_i and Q_i), and the sum of the wavefront aberration coefficients of the posterior corneal surface and lens surfaces. Some of the parameters are collected directly by different clinical instruments in pre-surgical measurement while the others require derivation from the model data. The asphericity and radius of corneal curvature can be derived from topography measurements. The refractive error (defocus) is measured by traditional aberrometry, such as an autorefractor. The sum of the aberration coefficients can be derived from the corneal topography data and from the wavefront aberration coefficients for primary spherical aberrations measured by clinical aberrometry.

At the time when Manns's work was reported, the method was still in its experimental stage. It can be seen from the provided Equations (3-21) to (3-24) of ablation profile calculation, that only defocus and primary spherical aberration are taken into account. Although the authors stated in their discussion that there will be further developments

to extend the formula's application to other aberrations, this part of work has not been published as yet.

Klein's Wavefront-only Approximation and Mrochen's Method

Klein's wavefront-only approximation was the first reported method adopting the entire Hartmann-Shack (HS) data to generate ablation profiles for comprehensive aberration correction.

At the beginning of Klein's work, he included both HS data and corneal topography to develop the proposed ablation profile algorithm for wavefront-optimized operation. However, in the latter approach without the corneal shape information, it was found that omitting the factors related to topography in the exact formula only introduced a neglectable error. A comparison of the ablation amount obtained from the exact and approximated algorithm is implemented, which shows the maximum difference of only 0.05 μm, that can be ignored while compared to the maximum ablation depth of approximately 60 μm for correcting a –5 diopters myopia (Klein, 1998).

The final form of Klein's approximated formula (3-17), can be decomposed into two parts: the ablation profile from HS wavefront data:

$$D_1(x,y) = [\max(W) - W(x,y)]/(n-1)$$

and the adjustment factor derived from the geometrical setting of wavefront measurement

$$D_2(x,y) = d\theta^2/(2(n-1) \approx d(0.003 * d)^2/(2(n-1))$$

which in fact brings little influence to the ablation profile for small amount of correction and optical zone. For a -10 diopters correction with a 6 *mm* optical zone, the adjustment amount is only 0.03 μm, while the maximum ablation depth is approximately 100 μm (Klein, 1998).

The required input parameters are wavefront data and refractive index of cornea. Correction in diopters will only be used for extreme cases. The wavefront data can be measured with standard HS wavefront sensor, and the refractive index of cornea is always taken as 1.376.

However, to deliver the complex ablation pattern for customized refractive surgery, higher requirements are raised for laser systems using a smaller beam size and more flexible scanning algorithms. Based on Klein's approximation method, Mrochen (2004) further simplified the formula for calculating wavefront-optimized ablation profiles, because the adjustment factor has little influence even for a large amount of correction with an optical zone covering most of the cornea. This formula can be seen as the improved form of the Klein's approximation formula. The new formula given by Equation 3-18 is completely independent of adjustment factors.

Summary

From the available ablation profile methods and their characteristics compiled in Table 4.1, it is clear that Klein's approximated formula and Mrochen's simplification support correction of both LOA and HOA. Thus, Klein's formula gives a direct prediction of ablation profile for comprehensive wavefront aberration correction, while requiring only the wavefront information (adjustment factor is not required for normal cases). One of the advantages of Klein's formula is the utilization of a single clinical instrument and there is no need to correlate wavefront and corneal topography measurements, which are required by most wavefront-optimized techniques based on topography data. On the contrary, the other methods require more parameters, which can not be directly measured, and lack of ability to correct HOA. Although there are higher requirements of related hardware systems for Klein's method than other methods, new developments in high precision laser systems and scanning algorithms will soon settle the problem. The advantages make Klein's approach the only candidate for a computerized study of the effectiveness of wavefront-optimal corneal ablation algorithms that encompasses the correction of all lower and higher order aberrations.

Table 4.1 A comparison of ablation profile methods

	Aberrations Corrected		**Parameters Required**	**Requirement for Laser System**
	LOA	HOA		
Munnerlyn's Approximated formula	Defocus	No	OZ, $D_{1,}$ (R_1 for exact formula)	Broad beam (2 *mm*) system with simple delivery algorithm
Manns's Method	Defocus	Primary spherical aberration	D_1, R_1, $Q_{1,}$ $W_{1,}$ W_2, W_3, W_4	Small beam (<=1 *mm*) system with simple delivery algorithm
Klein's Approximated Method	Defocus and astigmatism	Yes	HS Wavefront data (W)	Small beam (depends on aberration removal) system with complex scanning algorithm
Mrochen's Method (Simplified Klein's Method)	Defocus and astigmatism	Yes	HS Wavefront data (W)	Small beam (depends on aberration removal) system with complex scanning algorithm

Chapter 5

Evaluation of the Wavefront Only Corneal Ablation

Wavefront-guided refractive surgery is currently the most popular method used to improve the vision of eyes with optical irregularity. It has the potential to not only eliminate sphero-cylindrical refractive errors but also to reduce the higher order aberrations (HOA) of the eye (Huang, 2002; Mrochen *et al*., 2004 b).

There are three necessary components to achieve comprehensive aberration correction. They include a method of accurately measuring and mapping the total aberrations, an algorithm calculating the ablation profile from the aberration map, and a method to deliver the laser pulse according to the desired ablation profile (Huang, 2002). The introduction of Hartmann-Shack (HS) wavefront sensor technology has successfully addressed the problem of high-precision aberration mapping, while wavefront-guided laser delivery has greatly improved the accuracy of laser pulse control. In view of this, the demand for a practical method to calculate the comprehensive ablation profile has become obvious.

In this chapter, a simulation program based on the Klein's approach is developed to theoretically evaluate the effectiveness of this method in eliminating ocular aberrations including defocus, astigmatism and HOA. This is done by quantifying the changes in the wavefront error and visual Strehl ratios before and after a simulated ablation using clinical HS wavefront sensing data and videokeratoscope corneal

elevation maps of real patients. The effect of typical ablation alignment errors in refractive surgery on predicted visual outcomes was also examined.

5.1 Subjects and methods

Data from twenty-two eyes of 11 subjects, aged 18-36, were used for the study. There were 14 myopic eyes (<0.75 D cylinder), 6 eyes with myopic astigmatism, and two with mixed astigmatism (see Table 5.1).

All subjects underwent refraction in low luminance conditions using a Bailey-Lovie acuity chart. Following this, a Hartmann-Shack wavefront sensor (COAS, Wavefront Sciences, Inc.) was used to measure the total wavefront aberrations for each eye. To minimize the error caused by accommodation microfluctuations (Collins *et al*., 1995; Iskander *et al*., 2004), 25 consecutive wavefront measurements at frequency of about 10 Hz were taken for each subject's eye. Finally, the topographic data of the corneal surface was collected by a videokeratoscope (Keratron Optikon). Six topography measurements were taken for each eye, from which one was selected for analysis. The selected videokeratograph had clear Placido disk rings and clear pupil outline (Fogla and Rao, 2000; Wachler and Krueger, 2000). The coordinates of the pupil center (R,θ) with respect to the videokeratoscopic analysis axis (VK pupil offset) were recorded in order to match the topography data with the wavefront sensor data acquired at the line-of-sight, which was assumed to be the center of the pupil. The study met the requirements of the university Human Ethics committee.

Additionally, retrospective measurements of total wavefront aberrations of 20 age-matched emmetropic eyes were used as a benchmark in the analysis of optical effects of corneal ablation. The retrospective data were acquired with the same Hartmann-Shack sensor and the same lighting conditions that used for measuring the wavefront of the 11 patients.

Table 5.1 The subjects used in the study.

Subjects	**Low Luminance Spec Rx**			**VK Pupil Offset**	
	Sphere	Cyl.	Axis	R [mm]	θ [deg]
S1_OD	–4.50	—	—	0.295	250
S1_OS	–5.00	–0.25	90	0.301	272
S2_OD	–5.00	–0.50	20	0.141	168
S2_OS	–5.00	–0.25	10	0.155	320
S3_OD	–1.75	–0.25	90	0.673	179
S3_OS	–1.75	–0.25	90	0.603	356
S4_OD	–3.00	–0.25	180	0.328	179
S4_OS	–2.75	–0.50	165	0.257	345
S5_OD	–1.75	–0.25	110	0.331	208
S5_OS	–1.75	—	—	0.226	318
S6_OD	–0.25	–1.25	170	0.340	193
S6_OS	–1.00	–0.75	5	0.199	333
B7_OD	–3.50	–1.00	90	0.481	184
S7_OS	–4.75	–0.25	90	0.394	348
S8_OD	–3.50	–0.50	70	0.446	192
S8_OS	–3.75	–0.50	135	0.326	355
S9_OD	–3.50	–1.25	95	0.453	210
S9_OS	–5.00	–0.75	100	0.478	329
S10_OD	–3.00	–1.00	150	0.346	211
S10_OS	–4.50	–0.50	65	0.243	305
S11_OD	+1.00	–2.50	25	0.687	189
S11_OS	+0.50	–2.25	165	0.490	348

5.2 Computer simulation

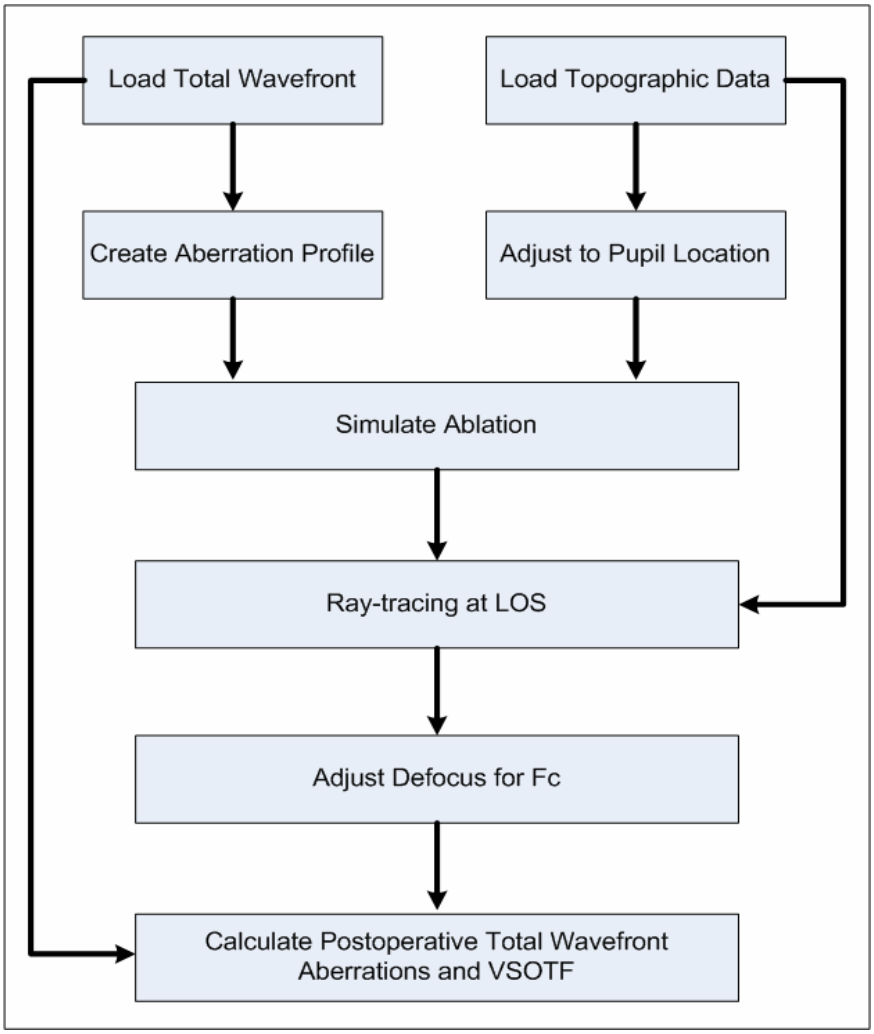

Figure 5.1 Flow chart of computer simulation procedures.

The simulated ablation of corneal surfaces based on Klein's approximated formula , see Equation (3-17) in Chapter 3, and all subsequent routines such as corneal ray tracing and calculation of optical and visual effects of the ablated cornea have been programmed from first principles in Matlab (The MathWorks, Inc.). An ideal laser beam with an infinitely small beam size capable of removing the desired amount of tissue was assumed. For this reason, there should not be any aberrations produced by residual tissue, which is always seen in procedures with a finite size of laser beam (Buzard and Fundingsland, 1997; Shimmick *et al*., 1997; Huang, 2002; Guirao *et al*., 2003). The flow chart of the computer simulation is shown in Figure 5.1

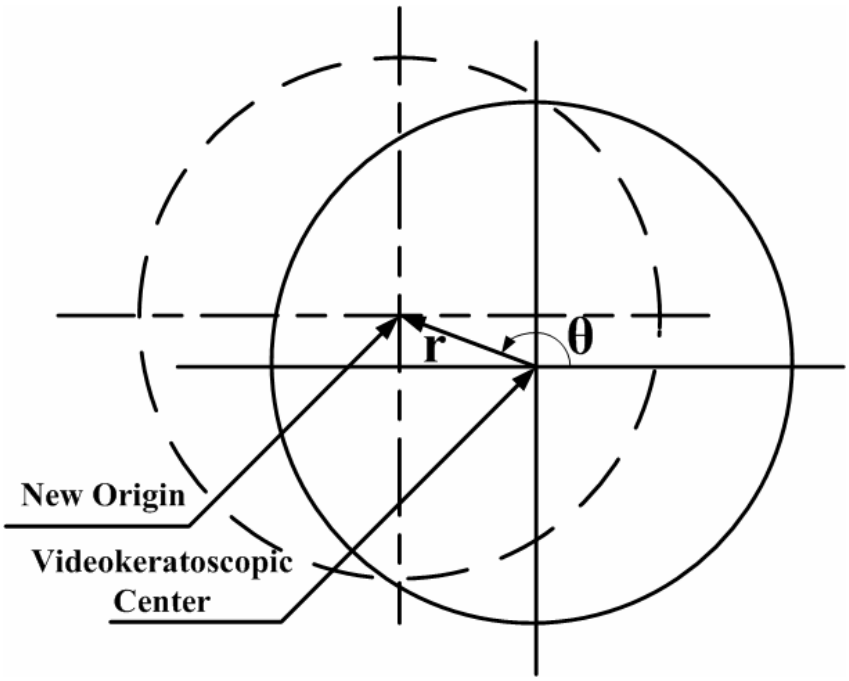

Figure 5.2 Pupil Offset Adjustment.

First, the Hartmann-Shack data of the total wavefront aberrations are imported. The wavefront data consists of a set of the 8th radial order Zernike coefficients. Although, the wavefront data were acquired at natural pupil sizes which were normally greater than 6 *mm*. For consistency a 6 *mm* pupil diameter was used to calculate the ablation profile $D(x,y)$ as given in Equation (3-17). To simulate the ablation, the topography data are loaded into the program and translated to a new origin as given by the videokeratoscope (VK) pupil offset, which is illustrated in Figure 5.2, in order to match the topographic data with the wavefront sensor data.

This leads to an ablated "postoperative" corneal topography given by

$$Z_a(x,y) = Z_o(x,y) - D(x,y) \tag{5-1}$$

where $Z_o(x,y)$ is the original preoperative topography map.

It can be assumed that the wavefront aberrations of the internal eye remain unchanged before and after the ablation (Artal and Guirao, 1998; Macros *et al*., 2001; Mrochen *et al*., 2003). Thus, the pre- and post-operative total wavefront aberrations can be described as

$$W(x,y) = W_c(x,y) + W_i(x,y) \tag{5-2}$$

and

$$W_a(x,y) = W_{c,a}(x,y) + W_i(x,y) \tag{5-3}$$

with $W_c(x,y)$, $W_{c,a}(x,y)$ representing the wavefront aberration of the anterior corneal surface before and after ablation, respectively, and $W_i(x,y)$ the internal eye wavefront aberration. It is found that only $W(x,y)$ was directly measured using a Hartmann-Shack sensor.

In the next stage of the computer procedure, corneal wavefront aberrations for both original and ablated topography data were calculated. A 3-D ray tracing algorithm is carried out for a corneal refractive index of 1.376 and incident light wavelength of 555 *nm*. The right-handed cylindrical coordinate system (Klein, 1998), in which the cornea anterior surface is situated about the z-axis with the apex at the origin, is used. The optical path difference (*OPD*) is calculated as a difference between the optical path length of a given ray and the principal ray whose position is determined by the VK pupil offset. Then, the corneal wavefront aberration is calculated at the line-of-sight (as determined by the VK pupil offset) for a 5 *mm* pupil diameter. A power correction from the spectacle to corneal plane was performed assuming a distance between the planes of 13 *mm*. A smaller pupil size than that of the ablated region was chosen here to minimize errors in the periphery associated with fitting Zernike polynomials to wavefront aberrations. To be able to calculate the wavefront error of the internal ocular components, a 5 *mm* pupil diameter was resampled from the originally acquired wavefront aberrations. The final stage of procedure is to calculate a "postoperative" wavefront aberration, given by

$$W_a(x,y) = W_{c,a}(x,y) + \left[W(x,y) - W_c(x,y)\right] \tag{5-4}$$

5.3 Data analysis

All considered wavefront aberrations were restructured by a series of 8th radial order Zernike polynomial expansions. Two main descriptors of optical and visual quality were used to evaluate the effect of corneal ablation on vision. The root mean square (RMS) value of a wavefront derived from the Zernike polynomial coefficients (excluding the piston and tilts) is a popular descriptor of optical quality in the pupil plane (Marsack *et al*., 2004). However, a wavefront RMS may not necessarily well describe the visual impact of the aberrations because different aberrations affect vision differently (Applegate *et al*., 2002). In fact, it was found that the wavefront RMS does not always correlate well with visual performance measured subjectively (Cheng *et al*., 2004). Figure 5.3 demonstrates the visual impact from different aberrations of two simulated eyes with the same wavefront RMS value of 0.125 μm.

The wavefront of Eye1, as shown in Figure 5.3(a), including only horizontal coma, produces a slightly blurry image comparing to the original "E" letter illustrated in Figure 5.3(c). A more serious distortion is observed from the image of Eye 2, whose wavefront is consisted of complex HOA.

On the other hand, the visual Strehl ratio based on the optical transfer function (OTF) is currently considered the best descriptor of visual performance that can be directly derived from the wavefront aberrations data (Marsack *et al*., 2004).

The visual Strehl OTF based ratio is defined as

$$VSOTF = \frac{\int_{-\infty}^{\infty}\int_{-\infty}^{\infty} CSF_N(f_x, f_y) \cdot \mathrm{Re}\{OTF(f_x, f_y)\}\, df_x df_y}{\int_{-\infty}^{\infty}\int_{-\infty}^{\infty} CSF_N(f_x, f_y) \cdot OTF_{DL}(f_x, f_y)\, df_x df_y} \tag{5-5}$$

where $OTF_{DL}(f_x, f_y)$ denotes the diffraction limited optical transfer function, $CSF_N(f_x, f_y)$ is the neural contrast sensitivity function (Campbell and Green, 1965),

and (f_x, f_y) denote the spatial frequency coordinates. It should also be indicated that in the derivation of the optical transfer function, normative data for the amplitude of the pupil function (Stiles-Crawford effect) (Stiles and Crawford, 1933) was used. The modulation transfer functions (MTF) of Eye1 and Eye2 are shown in Figure 5.4.

VSOTF values based on higher order aberrations were calculated for both the original wavefront data and simulated “postoperative” wavefront.

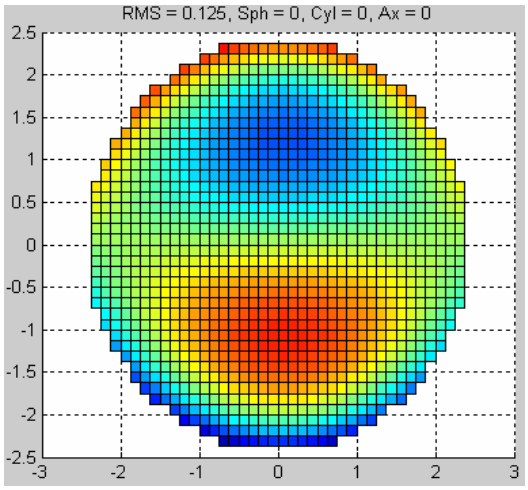

(a) Eye1 with only horizontal coma

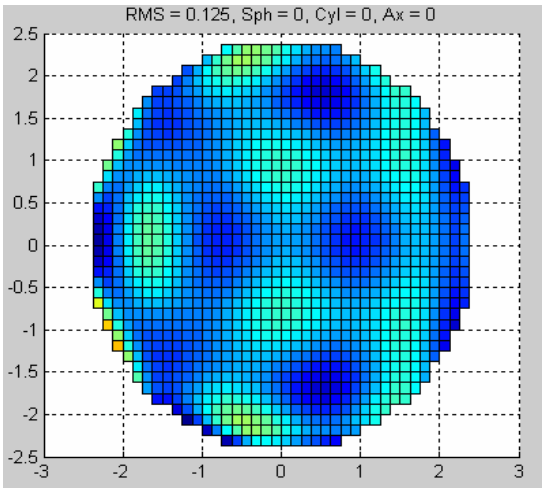

(b) Eye2 with complex HOA

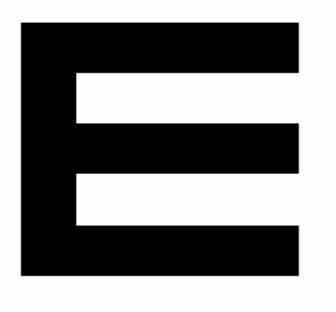

(c) Original E letter

(d) E letter image of eye1

(e) E letter image of eye2

Figure 5.3 Simulated impact of different aberrations on the vision performance.

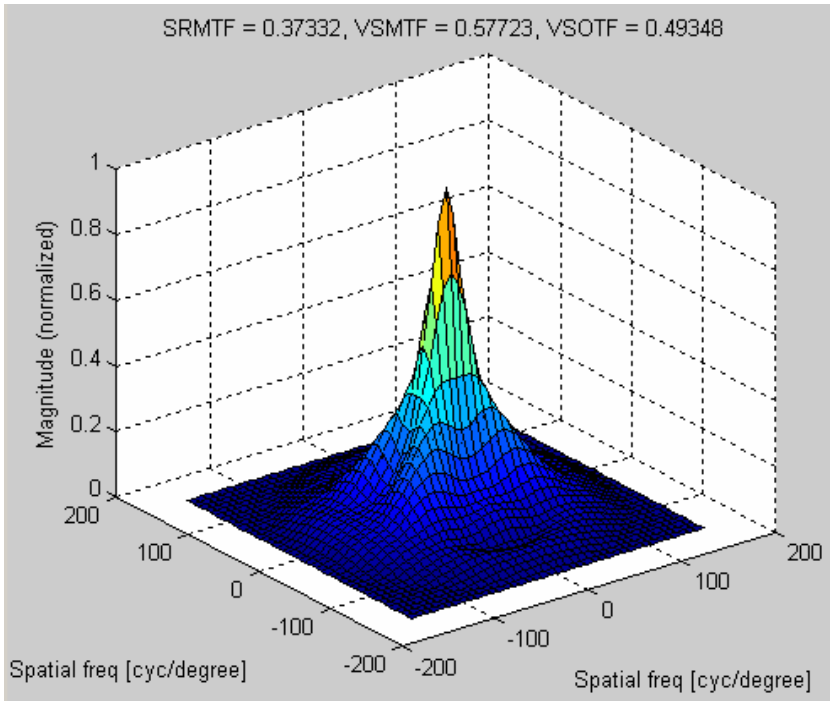

(a)

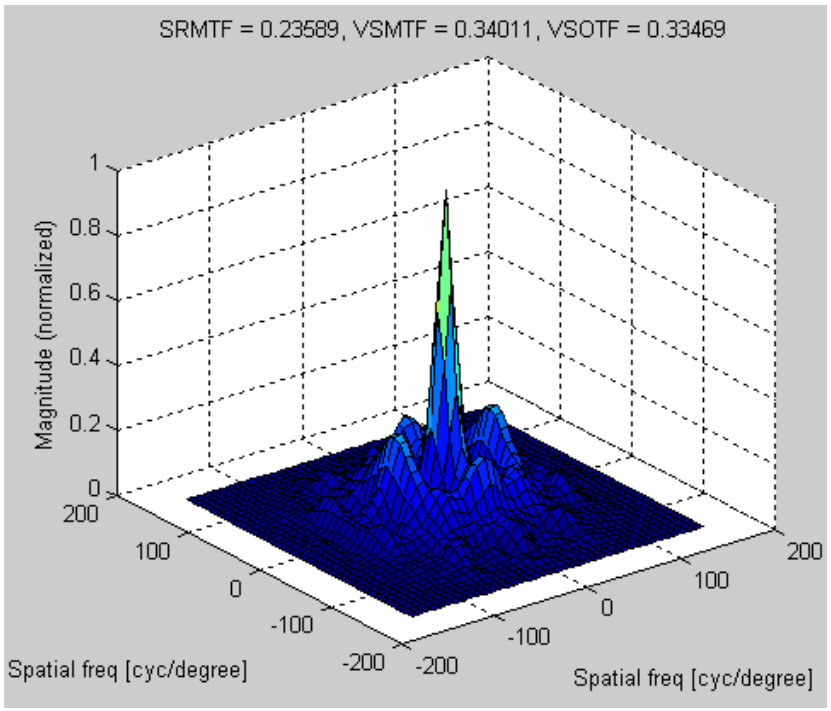

(b)

Figure 5.4 (a) MTF of Eye1. (b) MTF of Eye2.

5.4 Results

5.4.1 RMS of wavefront aberration

Figure 5.5 shows the RMS results of simulated correction for both total wavefront aberrations and higher-order aberrations alone (HOA).

Significant improvements in wavefront RMS for both total aberrations ($p < 0.001$) and HOA ($p = 0.0067$) are observed in all subjects except for the right eye of Subject 3, where the HOA wavefront RMS slightly increased from 0.101 μm to 0.120 μm. The average value of the "postoperative" higher order aberrations is reduced to about one third of the preoperative level. Total wavefront aberrations including lower and higher order aberrations decreased to about 4 % of the original value.

5.4.2 Visual Strehl ratios (VSOTF)

The visual Strehl ratios based on preoperative and "postoperative" higher order aberrations are shown in Figure 5.6.

On average the VSOTF value improved from 0.303 ± 0.16 (mean ± SD) to 0.782 ± 0.15 "postoperatively" and that improvement was significant, $p = 0.035$. However, the VSOTF of the right eye of Subject 3 showed the same trend (getting worse) as that of wavefront RMS, and dropped slightly from 0.608 to 0.554. Subject 3 had the largest VK pupil offset. However, this singular case cannot be generalized because no relation between the VK pupil offset and visual performance was found. Furthermore, different type of residual aberrations may response to the same degree of decentration differently.

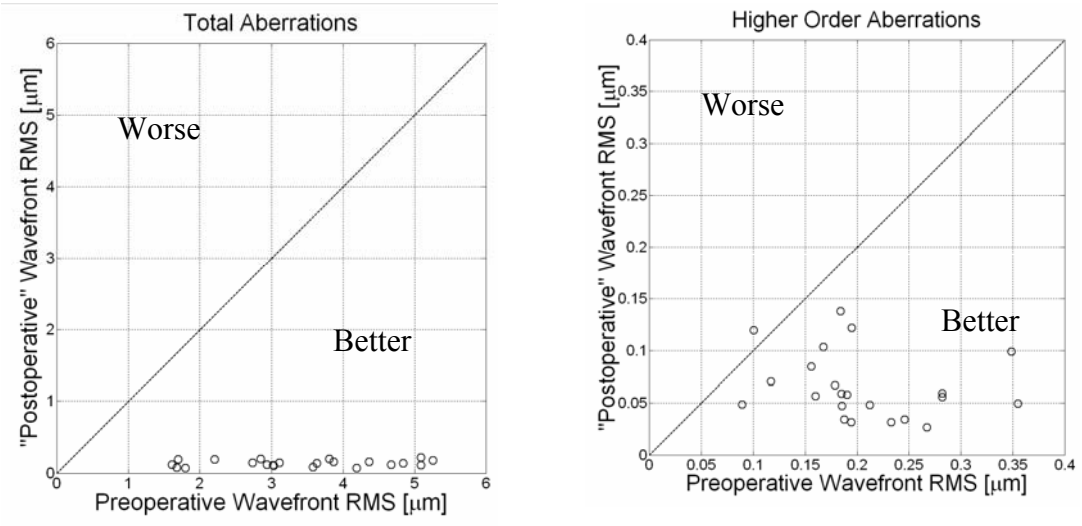

Figure 5.5 Pre- and "post"-operative wavefront RMS for total (left) and higher order (right) aberrations. The ablation procedure uses only total eye wavefront data (no corneal topography information) and assumes perfect ablation.

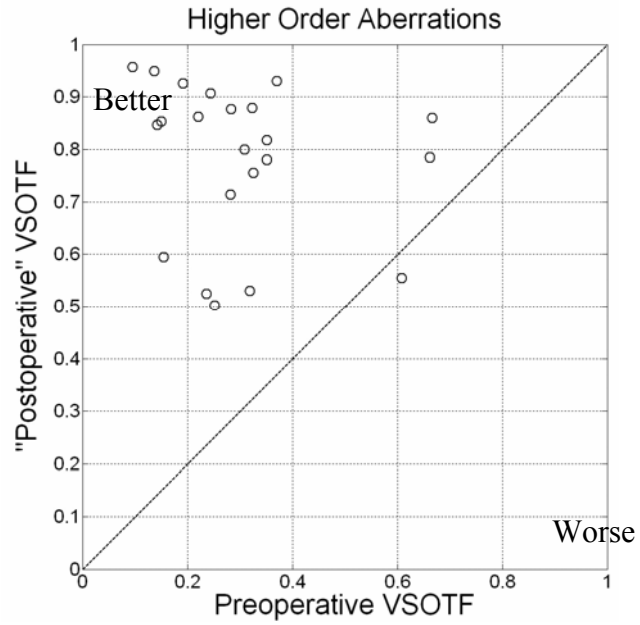

Figure 5.6 Pre- and "post"-operative VSOTF based on higher-order aberrations only and assuming perfect ablation.

5.4.3 Effect of decentration in surgical outcome

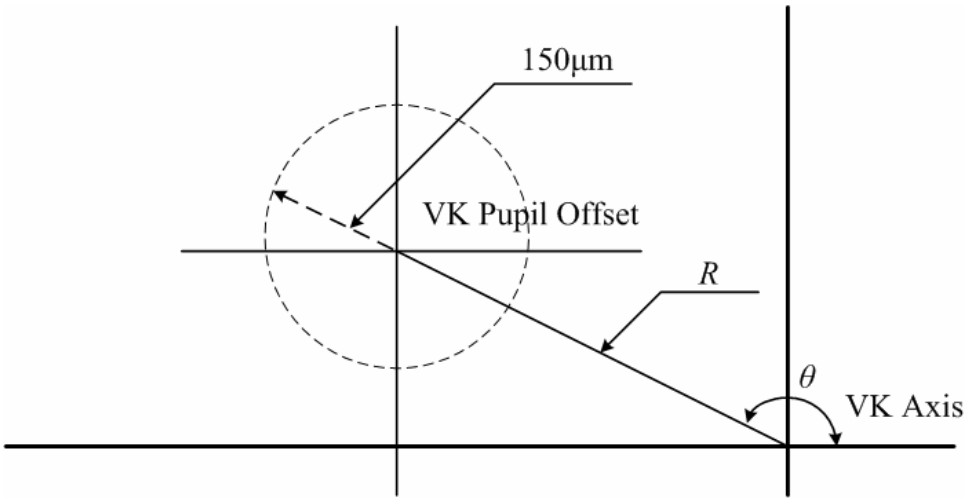

Figure 5.7 VK pupil offset with an additional 150 μm decentration in θ direction.

Several reports have pointed out that a decentration of the laser beam from the pupil center will produce significant changes in the ablated cornea that may affect visual outcomes (Mrochen *et al*., 2002; Bueeler and Mrochen, 2005; Donnenfeld, 2004). Typically, the laser beam may be decentered by about 60-70 μm and may reach up to several hundred microns (Bueeler *et al*., 2003). The effect of pupil decentration on visual correction by adding 150 μm to the measured VK pupil offset in the original direction of θ, which ensures the "worst case scenario" was studied. The concept of the additional pupil displacement is illustrated in Figure 5.7. Figure 5.8 shows the results of simulated correction for both total wavefront aberrations and HOA alone for a decentered VK pupil offset.

It is noted that even with a 150 μm decentration, a ten-fold improvement was recorded in "postoperative" total wavefront RMS, which drops to about 8.5 % of the preoperative value. However, the correction of higher order aberrations is less successful. In 6 out of the 22 eyes, the "postoperative" higher order aberrations RMS has increased. Nevertheless the average HOA wavefront RMS has dropped from 0.205 ± 0.069 to 0.156 ± 0.078 and that decrease in wavefront RMS was found to be significant ($p = 0.013$) . The visual Strehl ratios based on preoperative and "postoperative" high order aberrations for a decentered pupil are shown in Figure 5.9.

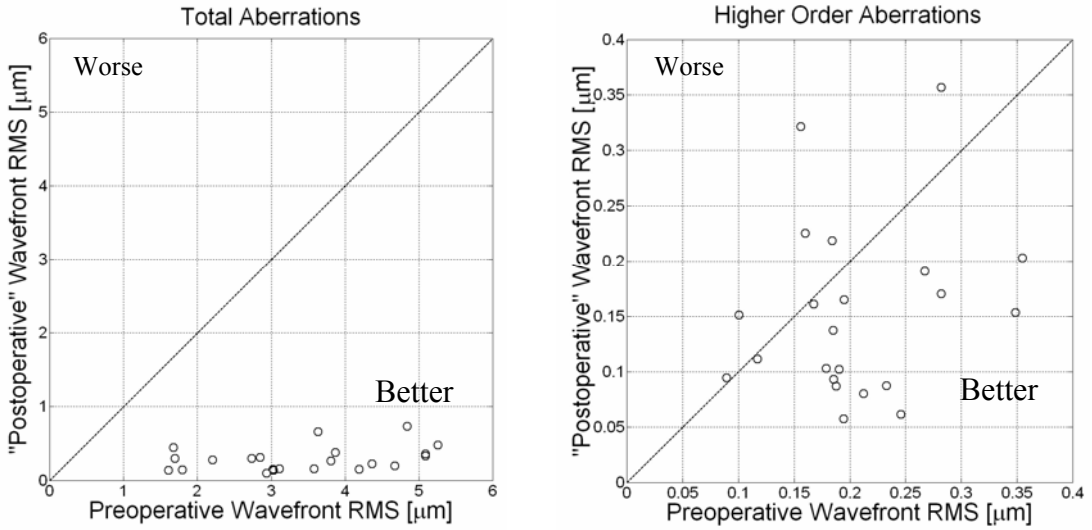

Figure 5.8 Pre- and "post"-operative wavefront RMS for total (left) and higher order (right) aberrations. The ablation procedure uses only total eye wavefront data (no corneal topography information) and assumes ablation misalignment of 150 μm.

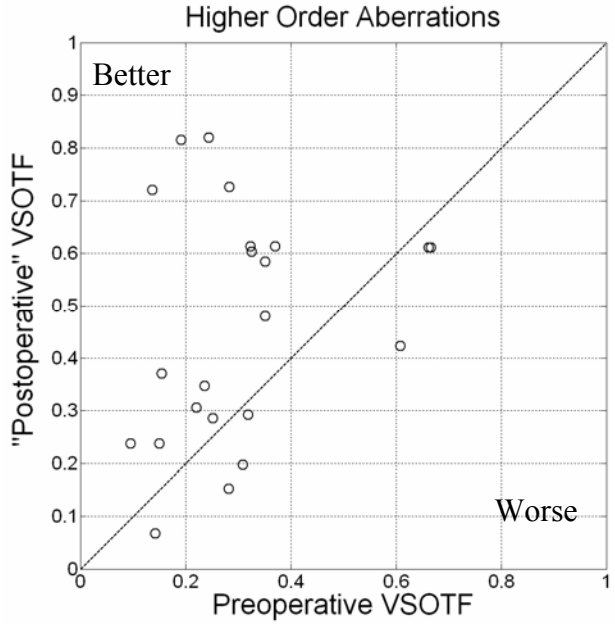

Figure 5.9 Pre- and "post"-operative VSOTF based on higher-order aberrations only and assuming ablation misalignment of 150 μm.

On average the VSOTF value slightly improved from 0.303 ± 0.16 to 0.459 ± 0.22 "postoperatively" and that improvement was again significant, $p = 0.0053$. Unlike for the HOA wavefront RMS, seven eyes for which the "postoperative" VSOTF decreased with respect to the preoperative ones were notived. However, no correlation was found between the trend in the VSOTF and the magnitude of the VK pupil offset.

Finally, the predicted visual outcomes were taken for a comparison, based on the group average VSOTF values, for the selected potential refractive surgery candidates to those of age-matched emmetropic subjects. It is noted that originally, the group average HOA based VSOTF for the candidates (0.303 ± 0.16) is significantly worse ($p = 0.0068$) than for the age-matched group of emmetropic subjects, where the VSOTF is 0.465 ± 0.20. "Postoperatively", the group average VSOTF of the "treated" group increased and that produced a significantly better visual outcome than that of the untreated emmetropes ($p < 0.001$). However, after additional 150 μm pupil decentration, the "postoperative" VSOTF became worse (0.459 ± 0.22) than that of untreated emmetropic subjects, and the change was no longer significant $p = 0.93$.

5.5 Summary

In Klein's paper, it was claimed that neglecting the corneal shape information introduces a negligible error in the optimal ablation depth of less than 0.05 ***μm***, while the maximum ablation depth for a –5 diopters myopic eye is often larger than 60 ***μm*** (Klein, 1998). However, in recent years uncertainty was raised about the application of optimal wavefront-only corneal ablation for patients with high-diopter refractive correction and those with significantly high amounts of HOA (Guell and Muller, 1996; Lee *et al*., 2003; Mrochen *et al*., 2004 b). In the author's study, seven eyes with relatively high refractive error (greater than or equal to –4.5 diopters) have shown good results in terms of predicted visual performance after the simulated ablation. Group mean of the total wavefront aberration RMS showed a 25-fold improvement while the HOA decreased to 34% of the original values. Significant improvements in both lower order and higher order aberrations were achieved in all but one subject.

Nevertheless, the VSOTF of higher order aberrations for this one particular subject was still comparable to that of original preoperative data.

It should be emphasized that in refractive surgery any predictions of visual performance should not be solely done on the basis of the ablation depth error, or equivalently on the wavefront RMS, and that metrics that correlate well with visual quality should also be used. Here the visual Strehl ratio based on the optical transfer function (VSOTF) was adopted as a predictor of visual performance (Cheng *et al*., 2004; Marsack *et al*., 2004). In case of higher order aberrations typically encountered in emmetropes, the VSOTF value ranges from 0.4 to 0.6. For the group of 20 age-matched emmetropes, an average value of 0.46 was obtained. However, for the refractive surgery candidates the group-mean VSOTF based on higher order aberrations exceeded 0.78 after simulated ablation. This indicates the possibility of achieving better VSOTF than that of the average emmetropic eye.

The simulated decentration of the pupil center by 150 μm showed slightly worse VSOTF but the change was found to be not significant when compared to the retinal image quality of emmetropes. Caution should be taken when comparing this result to that of Bueeler *et al.* (2003), who considered the decentration and its relation to the diffraction limited performance of the eye. Bueeler *et al.* (2003) show that decentration of the laser beam of 70 μm for a 7 *mm* pupil (or 200 μm for a 3 *mm* pupil) produces 5% decrease in the diffraction limited performance. The authors study shows that laser beam decentration of up to 150 μm (for 5 *mm* pupil) will not produce statistically significant differences to that normally found in emmetropes which is obviously much lower than the diffraction limited performance. Bueeler *et al.* (2003) compare their outcomes to a diffraction limited eye whereas the findings of the simulated procedures are compared to the natural level of performance derived from a group of emmetropic eyes providing a more realistic comparison of the results.

The theoretical study of wavefront-only corneal ablation showed variability in the results of "postoperative" wavefront RMS and VSOTF versus their preoperative values. This variability is attributed to real measurements of total wavefront aberration by the Hartmann-Shack sensor and real corneal topography elevations as well as the individual "structure" of higher order aberrations in each eye. It is

important, therefore, that corneal ablation procedures are not guided by a single measurement of wavefront aberration and that statistics of wavefront aberration measurements are taken into account. For example, an average of 25 consecutive wavefront aberration measurements sampled at around 10 Hz was used in the study.

As with any studies, there are limitations of the proposed methodology. An ideal laser with infinitely small beam size was assumed in our simulated ablation process. It removes any desired amount of tissue in the indicated location, which means that there is no ablation error due to residual tissue. Without an overlapping effect, it also brings a much smaller error compared to a larger spot size laser beam in case when a decentration of the laser beam from the pupil center occurs. The consideration of applying a laser beam of finite size and using a practical laser delivery algorithm will make the simulation more complex, but the outcome will provide a more realistic outcome. Recently Guirao *et al.* (2003) have investigated the effect of the laser beam on the benefits of customized refractive surgery. Another limitation of the proposed methodology is that biomechanical changes that may occur in the cornea during and after refractive surgery is not taken into account. That factor could be included by incorporating an average population response of the cornea. However, a customized correction may require an individual response to be accurate (Roberts, 2000). There are also other issues that limit the applicability of the proposed method, such as fixation during measurement and treatment, modeling wavefront aberration (reconstruction into a set of Zernike polynomials), changes in ablation profile (incident beam), scanning methods, eye tracking latency, and corneal healing (Mrochen and Bueeler, 2004). However, the implemented analysis does extend the work of earlier purely theoretical studies based on ideal ocular model, that do not take into consideration real topography and wavefront aberration measurements.

Also, the largest refractive error examined in the simulated procedure did not exceed –5 diopters. Cases with higher myopia and hyperopia as well as eyes with corneal irregularities such as keratoconus were not investigated. Finally, in data analysis, the pupil size was chosen to be 5 *mm* derived from an ablation zone of 6 *mm* diameter. This essentially limits the conclusions to photopic and mesopic lighting condition. Nevertheless, subjects with significantly larger pupils are usually screened out for refractive surgery (Holladay, 2002).

The subjects chosen to represent candidates are suitable for the LASIK procedure. The results of study on optimal wavefront-only corneal ablation methods indicate that, for the majority of clinical cases examined, the refractive surgery procedures that do not take into account the actual topography of the cornea will produce successful outcomes.

The presented methodology fills the gap between the theoretical work that is often based on mathematical models of corneal surface and diffraction limited criteria of visual performance that are unachievable in clinical practice (Manns *et al*., 2002; Bueeler *et al*., 2003) and the experimental work based on real clinical measurements. It provides the clinician with a screening tool that is based on real measurements of corneal topography and wavefront aberration of a particular patient. The software prediction of a deficient visual performance at this pre-surgical stage may expose, for example, inadequate measurement of wavefront aberration, axes misalignments, or unusual shape of corneal topography, prompting the clinician's attention. It would also provide some guidance on tolerances with respect to ablation alignment errors.

Although it may not be surprising that the ideal ablation based on wavefront measurement theoretically improves visual function, it is not certain that the ideal ablation based on real measurements of corneal topography and wavefront aberration will perform similarly well. For example, in the case of patient with keratoconus, where it is difficult to find the line-of sight, or for other patients with larger amount of higher order aberrations (post PRK, post-LASIK), the proposed methodologies may predict a deficient "post-surgical" visual performance. It is decided to include only data of subjects with normal corneas in the simulation study, as they are the great majority of those who undergo refractive surgery. Moreover, the methodology presented in the paper can be further enhanced in the future by adding the physical parameters of the laser beam, a complete laser scanning and locating method, biomechanical properties of the corneal surface, healing processes, etc.

Chapter 6

Potential Technologies of the Future

The traditional refractive surgery utilizing broad beam laser has been proved not capable to adequately correct higher order aberrations (HOA). On the contrary, additional HOA is observed in large amount of postoperative objects after the corneal smoothness is reduced (Manns *et al.*, 1995; Huang *et al*., 2003). The introduction of wavefront-guided LASIK technology significantly improves the surgical accuracy and provides the capability to remove HOA. However, the potential of modern LASIK technology to correct HOA is still restricted by a number of factors along with the LASIK procedures.

In this chapter, new developments of both hardware and software, which can be applied to improve the current ablation algorithm and scanning system, are reviewed in details. A concept of laser refractive surgery system utilizing the new technologies, which has the potential to overcome the limitation with the current LASIK technology, is purposed.

6.1 Design of an advanced laser scanning algorithm

In procedures using scanning laser devices, the laser beam with a spot diameter varying from 0.2 *mm* to 1 *mm* is moving on the corneal surface to remove desired amount of tissue on relative position. Comparing with the procedures adopting larger

laser beams, it provides a high predictability of postoperative visual outcome, which generated a considerable clinical interest. However, a great number of factors such as decentration, physical aspects of ablation, biomechanics of cornea, flap, wound healing and laser type influence the laser ablation procedures (Guirao *et al*., 2000; Chuck *et al*., 2001; Pallikaris *et al*., 2002; Bueeler and Mrochen, 2005) and prompt a visible difference between the expected result calculated by ablation equations and experimental data. Therefore, it is essential to quantify the influence of these parameters in refractive surgery in order to improve the surgical precision, especially for customized wavefront guided refractive surgery. A complex scanning algorithm should be developed adding adjustment factors that considering the influence of physical aspects such as the reflective energy losses, non-normal incidence and method of pulse overlapping.

6.1.1 Manns *et al.*'s scanning algorithm for corneal reshaping

An early algorithm for corneal reshaping with a scanning laser beam was developed by Manns *et al.* (1995) to determine the relationship of laser beam parameters, which include the ablation rate, beam intensity distribution, spot size and overlap ratio, and the surgical period and postoperative corneal smoothness. The block diagram of the algorithm is shown in Figure 6.1.

The tissue removed by a single laser pulse or ablation per pulse is given by the composition of the ablation rate and the beam-intensity distribution. The beam intensity distribution is assumed to be Gaussian, with a maximal radiant exposure of 400 mJ/cm^2, which has been proved to be a sufficient and safe exposure adopted by a large number of clinical processes (Krueger and Trokel, 1985). The other input parameters of the algorithm are the beam diameter, overlap ratio, diameter of the treatment zone, energy per pulse and the amount of tissue to be removed.

The relationship of laser parameters and duration of surgery is firstly identified. The hydration of cornea is changing during the laser treatment, which will greatly affect the ablation rate. A long surgical period also intensifies the discomfort of patients. For this reason, the ablation period must be controlled within a reasonably short time.

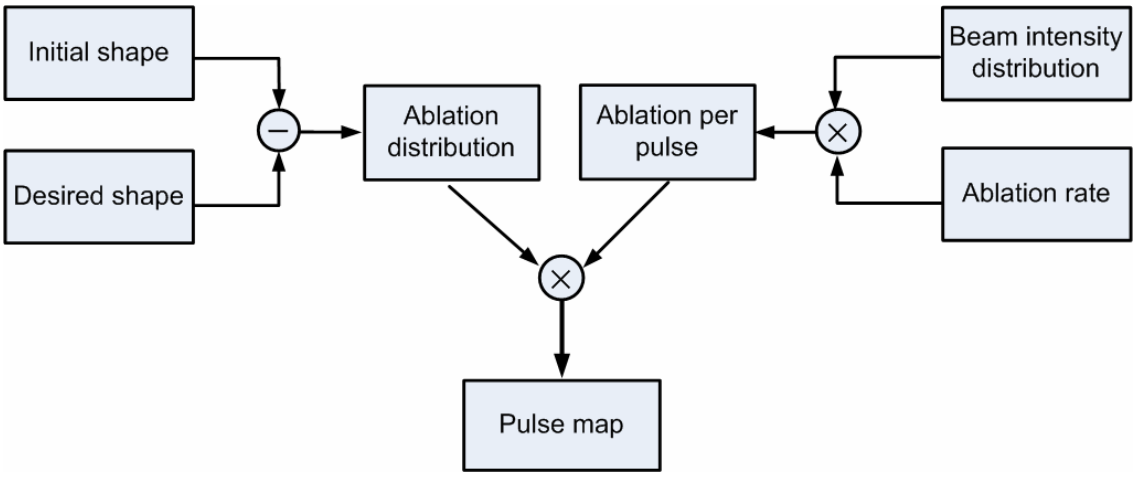

Figure 6.1 Algorithm for the calculation of the pulse-distribution map.

In an ideal condition, the duration of surgery is equal to the number of required laser pulses divided by the repetition rate of the laser. The number of laser pulses is estimated by the ratio of the total volume of removed tissue and the volume of tissue ablated by one pulse (Kurtz *et al.*, 1997). In Manns *et al.*'s research, the Munnerlyn formula is adopted to calculate the required amount of ablation. For a myopic case, the amount of tissue to be removed is equal to the subtraction of volume of a spherical cap with base diameter d and radius of curvature of the initial cornea (R_i) from the volume of a spherical cap with base diameter d and radius of curvature of the target corneal surface (R_f), given by

$$V = \frac{\pi}{64} d^4 \left(\frac{1}{R_i} - \frac{1}{R_f} \right) \tag{6-1}$$

After introducing the difference of refractive index at the air-cornea boundary ($\Delta n = 0.376$), the amount of ablation in Diopters, D_1, is given by

$$D_1 = \Delta n \left(\frac{1}{R_f} - \frac{1}{R_i} \right) \tag{6-2}$$

and Equation (6-1) becomes

$$V = -\frac{\pi}{64} \frac{d^4}{\Delta n} D_1 \tag{6-3}$$

The volume of tissue removed by a single laser pulse with the Gaussian profile can be approximated as

$$V_1 = \frac{\pi}{24} b^2 A \ln \frac{I_0}{I_{th}} \tag{6-4}$$

where b is the $1/e^2$ diameter of the beam, A is the peak ablation per pulse, I_0 is the maximum radiant exposure and I_{th} is the ablation threshold (Krueger and Trokel, 1985). If the peak radiant exposure is higher than the plateau radiant exposure ($I_0 > I_p$), the ablation per pulse can be further approximated as the volume of a truncated cone

$$V_1 = \frac{1}{3} \pi h (a^2 + ac + c^2) \tag{6-5}$$

in which h stands for the height of the truncated cone, a and c represent the radius of top and base respectively.

Then Equation (6-4) becomes

$$V_1 = \frac{\pi}{24} b^2 A \ln \frac{I_0}{I_{th}} \left\{ 1 + \frac{\ln(I_0 / I_p)}{\ln(I_0 / I_{th})} + \sqrt{\left[\frac{\ln(I_0 / I_p)}{\ln(I_0 / I_{th})} \right]} \right\} \tag{6-6}$$

where I_p is the plateau radiant exposure.

The number of required pulses is then given by

$$N = \frac{V}{V_1} = -\frac{3d^4 D}{8\Delta n b^2 A (1+\alpha) \ln(I_0 / I_{th})} \tag{6-7}$$

$$\alpha = \frac{\ln(I_0 / I_p)}{\ln(I_0 / I_{th})} + \sqrt{\left[\frac{\ln(I_0 / I_p)}{\ln(I_0 / I_{th})} \right]} \qquad \text{if } I_0 > I_p$$

It can be seen that using a larger beam size can significantly reduce the operation time. A higher peak radiant exposure will also shorten the duration of surgery. However,

increasing both of the values brings higher roughness on the postoperative corneal surface and reduces the surgical precision. An optimal balance between the laser parameters and operation period must be obtained.

For treatment of 5 *mm* ablation zone, for example, a result with acceptable residual refractive error and corneal roughness is achieved by applying a laser beam with a diameter less than 0.5 *mm* and an overlap ratio higher than 60% in Manns *et al.*'s model. The error after correction is estimated to be less than 0.1 diopter for correction up to 6 diopters, and less than 0.4 diopter for correction of 10 diopters. The corneal roughness is less than 6% of the central ablation depth, while the duration for correcting one dioptor is 25 seconds at a 100 Hz laser repetition rate (Manns *et al*., 1995).

The application of Manns *et al.*'s model in an ideal condition, which ignores the energy loss at periphery and the problem of spot locating, but provides a highly predictable visual outcome for treatment of spherocylindrical aberrations. However, disadvantages of the method are also obvious. Laser pulses are assumed to be applied to the cornea at predefined equally spaced position, which moves on only horizontal and vertical direction. The detail of beam overlap is also idealized to particular percentage. Moreover, due to the adoption of the Munnerlyn formula for calculating ablation profile, the correction of HOA is not considered.

6.1.2 Adjustment factor to compensate the energy loss at periphery area due to reflection and decrease of energy density

One of the known limitations of laser ablation predictability is the interaction between corneal shape and the effect of beam incidence angle on ablation efficiency. Moving a scanning laser spot from the center of the corneal surface to the limbus can result in an increase of illumination area and reflection energy loss, which leads to a decrease of ablation depth per pulse (Mrochen and Seiler, 2001; Jimenez *et al*., 2002), while the lower ablation depth per pulse brings changes to the shape of desired ablation pattern.

The modern refractive surgery using ultraviolet laser is based on the photoablation effect, which is known as a threshold process. Tissue removal only happens while the radiant exposure is higher than approximately 50 mJ/cm^2 (Krueger and Trokel, 1985). Photoablation caused by laser energy above the threshold value can be approximated by Lambert-Beer's law (Al-qahtani *et al*., 2001):

$$d_p = m \cdot \ln\left(\frac{F_0}{F_{th}}\right) \qquad \text{if} \quad F_0 > F_{th} \tag{6-8}$$

$$= 0 \qquad \text{if} \quad F_0 \le F_{th}$$

where d_p is the ablation depth per pulse, m is the ablation rate at $F = e \cdot F_{th}$, F is the incident exposure of the laser beam and F_{th} is the threshold value. Value of m and F_{th} were experimentally determined to be of 0.3 μm per pulse and 50 mJ/cm^2 (Krueger and Trokel, 1985).

Considering the 2-D condition in a spherical eye model, when the incident laser beam is delivered to the periphery spot at a distance r from the apex of anterior corneal surface with a radius of R, the incident angle will be

$$\theta(r) = \sin^{-1}(r/R) \tag{6-9}$$

The fluence value $F(r)$ of the laser beam delivered at a radial distance r is described by

$$F(r) = F_0 \cdot \cos(\theta) = F_0 \cdot \sqrt{1 - \frac{r^2}{R^2}} \tag{6-10}$$

in which F_0 stands for the maximum radiant exposure at the corneal apex, and the other variables are shown in Figure 6.2. Combining Equations (6-8), (6-9) and (6-10), the ablation depth related with the radial distance becomes

$$
\begin{aligned}
d(r) &= d_0 \cdot m \cdot \ln\left(\frac{F(r)}{F_{th}}\right) \\
&= d_0 \cdot m \cdot \ln\left(\frac{F_0}{F_{th}} \cdot \sqrt{1-\frac{r^2}{R^2}}\right)
\end{aligned}
\tag{6-11}
$$

where d_0 is the maximum ablation depth per pulse generated by normal incident laser beam at the corneal apex.

Moreover, the fluence of laser beam at the periphery of corneal surface is additionally affected by the increase of reflectivity. Taking this fact into account, Equation (6-11) becomes

$$
d(r) = d_0 \cdot m \cdot \ln\left(\frac{F_0}{F_{th}} \cdot \sqrt{1-\frac{r^2}{R^2}}\right) \cdot (1 - refl(r)) \tag{6-12}
$$

where $refl(r)$ is the reflectivity at a point with a radial distance r from the corneal apex. In Ginis *et al.*'s (2003) research, the reflectivity of air-cornea interface is defined as

$$
refl(r) = \frac{Q_s^2 + Q_p^2}{2} \tag{6-13}
$$

according to the Fresnel's law for reflection (Zhang, 1977). The sagittal (Q_s) and parallel (Q_p) polarization amplitude coefficients of reflection are calculated by

$$
Q_s(\theta) = \frac{\sqrt{n^2 - \sin^2(\theta)} - \cos(\theta)}{1 - n^2}
$$

$$
Q_p(\theta) = \frac{n^2 \cos(\theta) - \sqrt{n^2 - \sin^2(\theta)}}{n^2 \cos(\theta) + \sqrt{n^2 - \sin^2(\theta)}}
$$

where θ is given by Equation (6-9). A value of 1.52 for the corneal refractive index n at 193 *nm* is adopted (Jimenez *et al.*, 2002).

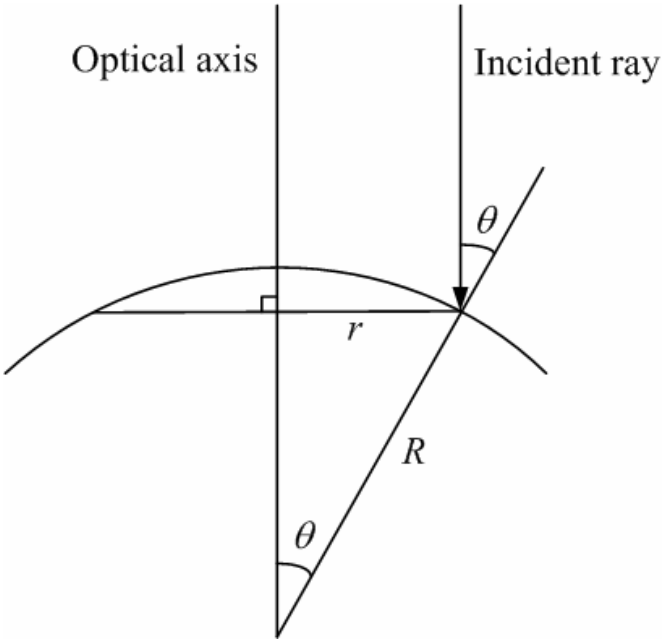

Figure 6.2 Schematic representation of a non-normal incident laser beam.

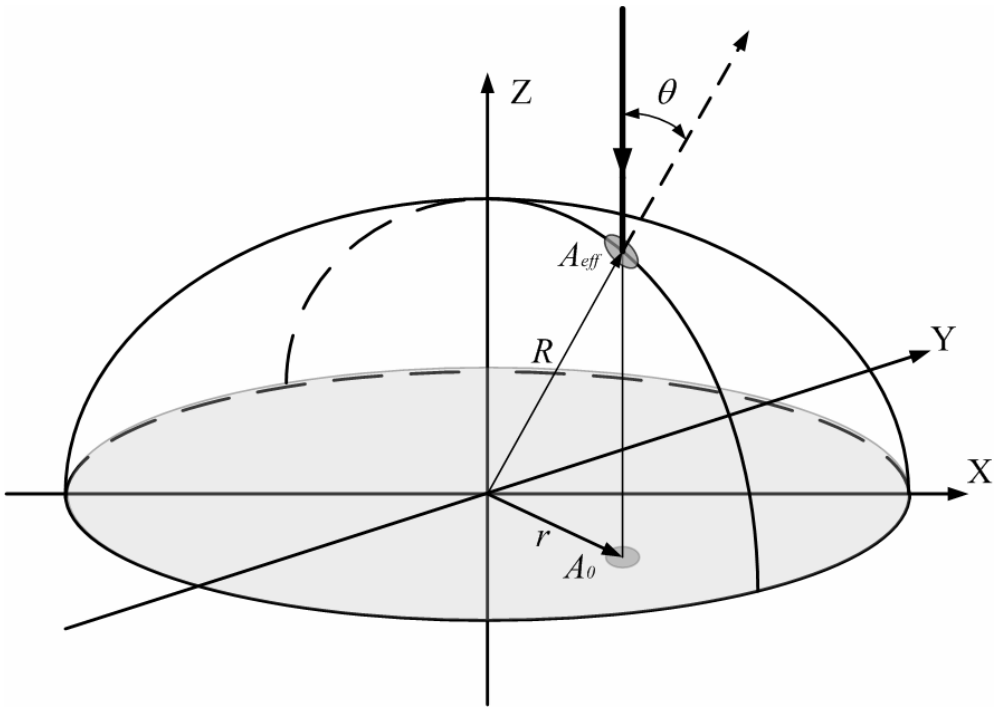

Figure 6.3 Effective illumination area on the corneal curvature surface.

Considering the effect of laser beam size (*r*s), which is one of the main factors in correcting HOA, a more complex 3-D model is obtained as Figure 6.3.

The effective illumination area A_{eff} is estimated at the first place, which can be mathematically derived from the projection of a circular spot A_0 on the X-Y plane onto the corneal curvature surface as shown in Figure 6.3. The effective illumination area A_{eff} at location with a radial distance $r = \sqrt{x^2 + y^2}$ to the corneal apex is calculated by

$$A_{eff}(r) = \int_{-rs}^{rs} \int_{-\sqrt{rs^2 - x^2} + r}^{\sqrt{rs^2 - x^2} + r} \sqrt{1 + \left[\frac{\partial}{\partial x} f(x,y)\right]^2 + \left[\frac{\partial}{\partial y} f(x,y)\right]^2}\, dxdy \qquad (6\text{-}14)$$

Relative change of effective illumination area, which is required for estimating the compensation factor, is given by

$$k_1(r) = \frac{A_{eff}(r)}{A_0} = \frac{A_{eff}(r)}{\pi r s^2} \qquad (6\text{-}15)$$

where $A_0 = \pi r s^2$ is the illumination area produced by normal incident laser beam.

The reflection losses in 3D can be calculated from Equation (6-13)

$$k_2(r) = \frac{Q_s^2 + Q_p^2}{2}$$

Combining Equations (6-12), (6-13) and (6-15), ablation depth related with the radial distance *r* as well as the influence of non-normal incidence and reflectivity is expressed as

$$d(r) = d_0 \cdot m \cdot \ln\left(\frac{F_0}{F_{th}} \cdot k_1(r)\right) \cdot (1 - k_2(r)) \qquad (6\text{-}16)$$

which can be applied in ablation pattern calculation to compensate the laser energy losses at periphery corneal area.

6.1.3 Correction factor of overlap with Gaussian-profile beams

It is known that the finite size of laser beam limits the ablation accuracy and it causes a problem of pulse overlapping in procedures using scanning laser. Most of the conducted researches about the overlapping methods are based on Gaussian beams, which are adopted by most lasers used for refractive surgery (Iseli *et al*., 2004; Jimenez *et al*., 2005). A primary study on the effect of overlap ratio to the postoperative corneal roughness and ablation period has been fulfilled by Manns *et al.* (1995). Their research has numerically simulated that a higher overlap ratio can achieve a better corneal smoothness, at the same time the ablation period is extended. Recently, a correction constant has been proposed by Jimenez *et al.* (2005) to analytically quantify the overlapping effect, which can be applied to any current ablation algorithms using Gaussian beams.

The exposure of a Gaussian beam is described as

$$F(x,y) = F_0 \exp\left[-2(x^2+y^2)/w^2\right] \tag{6-17}$$

where x and y are the special coordinates, w is the beam radius and F_0 is the peak exposure. A point on the cornea affected by overlap pulses is shown in Figure 6.4.
The exposure is limited to a spot size of b.

A correction factor for the ablation depth per pulse, c, that takes into account the overlapping effect can be defined as

$$c = \frac{\int_0^{r'} m \cdot \ln\left(\frac{F_0 \exp\left[-2(x^2+y^2)/w^2\right]}{F_{th}}\right) dxdy}{\int_0^{r'} m \cdot \ln\left(\frac{F_0}{F_{th}}\right) dxdy} \tag{6-18}$$

where F_{th} is the threshold value of photoablation exposure. Value of m and F_{th} were experimentally determined to be of 0.3 μm per pulse and 50 mJ/cm^2.

It calculates the contribution to the photoablation due to exposure at the overlap area. The value of exposure received from surrounding pulses depends on the distance according to the given Gaussian function as Equation (6-17). Therefore, the total irradiance can be easily calculated by integrating the contribution of surrounding points with a radius r', which depends on the spot size b, and the radial distance r where the ablation is located.

According to the photoablation process defined by Equation (6-8), r is obtained by

$$r = \frac{\sqrt{2}}{2} w \left(\ln \frac{F_0}{F_{th}} \right)^{1/2} \tag{6-19}$$

Thus the integral range in Equation (6-18) is limited as $r' = \min \{r, b/2\}$. For an uniform beam ($w = \infty$), the value of c is 1. Since Equation (6-18) can be rewritten as

$$c = \frac{m \int_0^{r'} \left(\ln \left(\frac{F_0}{F_{th}} \right) - 2 \frac{x^2 + y^2}{w^2} \right) dxdy}{m \cdot \ln \left(\frac{F_0}{F_{th}} \right) \int_0^{r'} dxdy}$$

When $\int_0^{r'} dxdy = \pi r'^2$ and $\int_0^{r'} (x^2 + y^2) dxdy = \pi r'^4 / 2$, the above equation becomes

$$c = 1 - \frac{r'^2}{w^2} \left(\ln \frac{F_0}{F_{th}} \right)^{-1} \tag{6-20}$$

The obtained correction factor takes into account the parameters of a Gaussian beam including w, spot size b and exposure. The effectiveness of factor c is theoretically examined by applying it with the ablation algorithm on the corneal surface modeled by a conicoid function. And it is found that the introduction of correction factor c greatly improves the predictability of visual outcome in procedures using Gaussian profiled lasers (Jimenez *et al*., 2005).

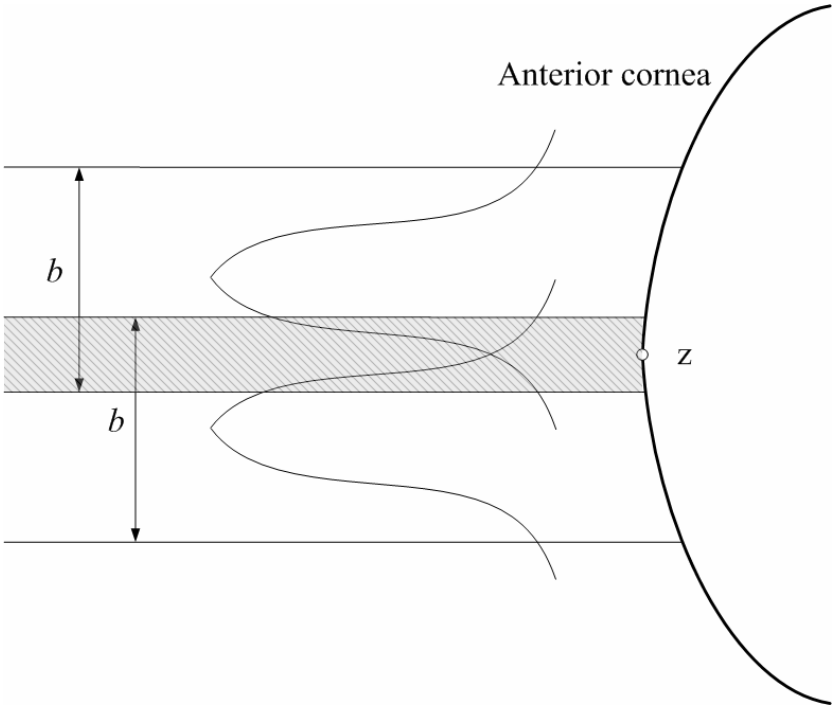

Figure 6.4 Effect of overlapping due to finite-size of the incident beam.

6.2 Technologies of real time laser beam shaping

The influence of beam size on correction of different types of aberrations is well discussed in preliminary researches (Huang, 2002; Guirao *et al*., 2003). Theoretically, a laser beam with infinitely small beam size is capable to remove the whole range of aberrations. The laser beam with a diameter of 0.1 mm can correct up to the 4th radial order of Zernike aberrations (Huang, 2002). However, the surgical time is also increased when a smaller laser beam is used.

Most of the currently marketed laser equipments for refractive surgery are working on predetermined beam size mode, which remains unchanged during the surgical process. An obvious problem for using fixed beam size laser is the increase of energy losses at the periphery area as indicated in Figure 6.5, which requires more complex compensation to overcome the decrease of illumination energy density.

The use of variable beam size in scanning laser technology is suggested to be the proper solution to achieve a good balance between surgical time and vision

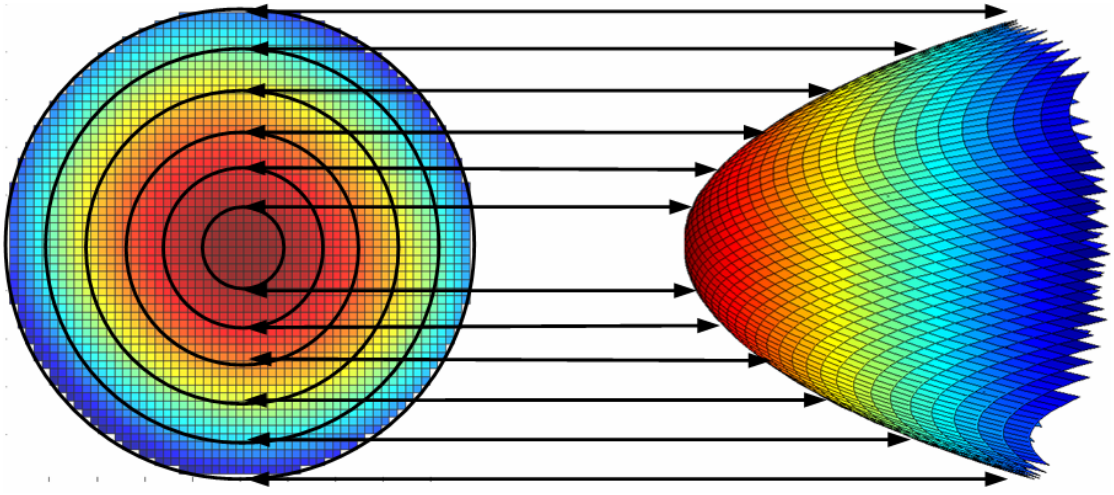

Figure 6.5 Increase of energy losses at periphery area using fixed beam size laser.

improvement. A laser beam with larger beam size can be applied first to remove the low order aberrations. Then the laser beam size deceases dynamically when correcting the HOA.

The described functions are based on a flexible laser shaping technology in a dynamic condition. Three possible methods of real-time beam shaping have been considered in this study. They are: 1) optical displacement elements, 2) multi-spots Technique, and 3) Digital mirror devices (DMD).

6.2.1 Beam shaping by using optical displacement elements

According to Komazaki *et al*. (2003), a method of beam shaping by using an optical displacement sensor having a semiconductor laser light source provide a new idea of beam shaping technology. The structure of the optical displacement sensor is shown in Figure 6.6. z_1 and z_2 indicate the distance from the reflecting grating to the laser source and the substrate respectively.

As presented in the figure, by adjusting the diffuse angle φ of the emitting laser beam and changing the pitch distances and relative directions of the reflecting grafting, the outcome beam shape and size are changed on the receiving layer. Transmission grating located in the laser source and reflecting grating are the most important

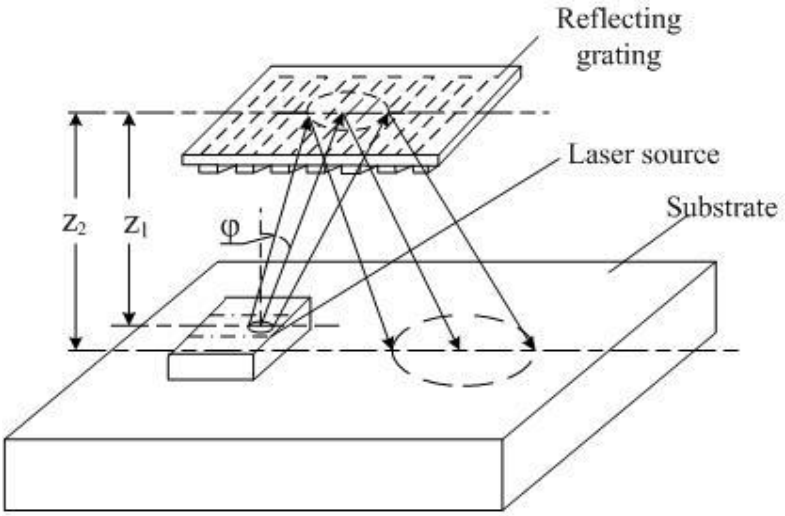

Figure 6.6 Structure of the optical displacement sensor.

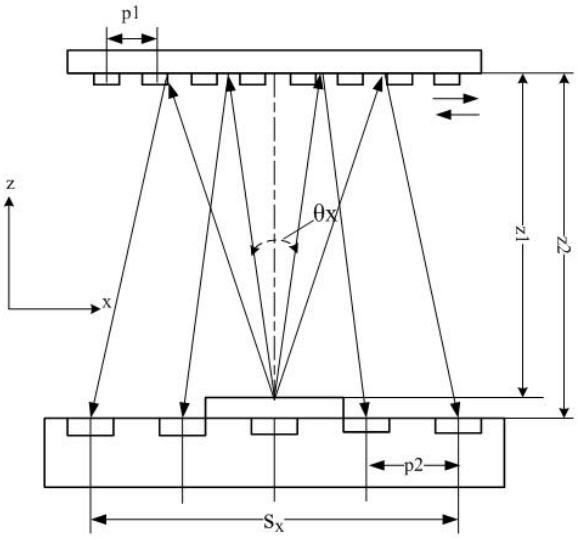

Figure 6.7 Optics of the optical displacement sensor.

components in its optical path. Figure 6.7 represents the section of the optics in vertical direction of *x*-*z* plane. p1 and p2 are the pitch distances of the reflecting gratings and the substrate, while s_x represent the beam size on the received layer.

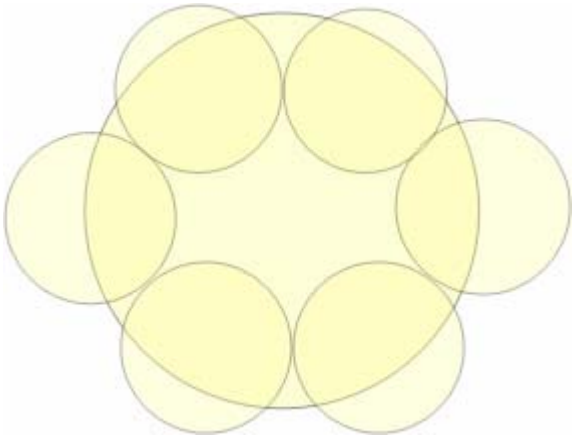

Figure 6.8 An approximated elliptical spot composed by 7 spots.

6.2.2 Multi-spots technique

The second method of interest is the variable spot scanning technique that could be developed for more accurate ablation process. In spite of the improvement on optic control, it adopts the multi-sport technique to achieve a flexible beam shaping. In this case, the laser beam is composed of seven overlapping beams forming a required beam shape and smoothing the edge of ablation (Shimmick, 2001) as shown in the figure 6.8.

The multiple spots technology is currently applied on VISX STAR S3 Excimer Laser system developed by ALCON USA. The spot size various from 0.65 *mm* to 6.5 *mm*, which is sufficient for eliminating the regular sphere-cylindrical aberration and some of higher order aberrations.

6.2.3 Beam shaping by using digital mirror devices

The third choice is described in US patent No. US 6,394,999 (Williams *et al*., 2002). It is a technique of programmable light beam shaping using digital mirror devices (DMD). Configuration of one micro-mirror in the instrument is displayed in Figure 6.9. A typical micro-mirror in digital mirror device (DMD) system is simply an on/off device. Figure 6.10 gives more details on the working optical path.

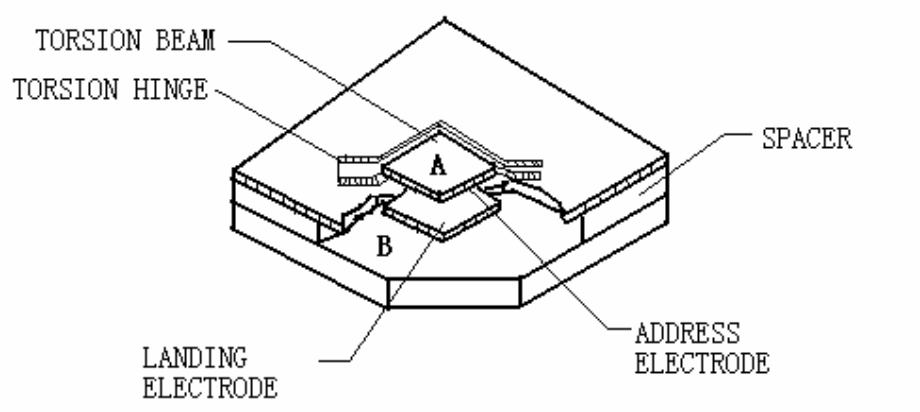

Figure 6.9 Configuration of the Micro-mirror.

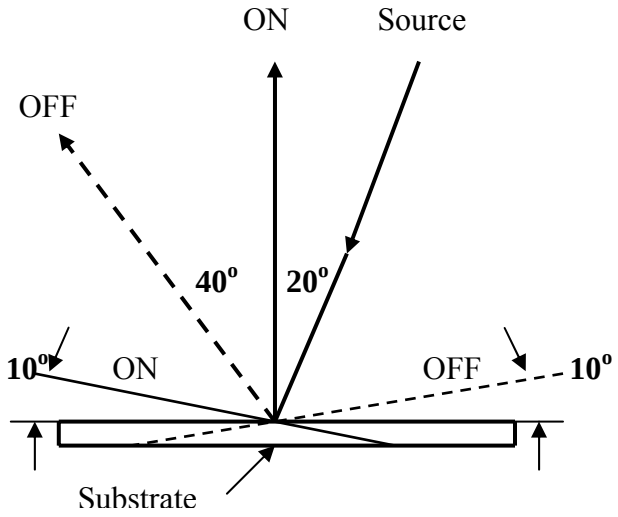

Figure 6.10 Optics of a Micro-mirror.

For the “on” state, when the incidence angle is less than 20 degree, the source beam will be reflected to the pre-fixed direction. If the base of an element micro-mirror tilts a 10-degree angle, the incidence angle will be now 40 degree, and the source ray is diffuse reflected. From the direction of illuminated object, the micro-mirror shows as dark. The target area receives nothing from this part of source beam in this case.

After detailed comparison among the beam shaping methods, due to the unique advantages, beam-shaping technology using DMD is adopted for the optimization of pulse delivery system. As mentioned above, digital mirror devices have the particular features meeting the requirements for high-precision pulse delivery.

i) High switching speed

Controlled by an electric base, each micro-mirror element can finish the programmable on/off switch within 10 Fs (Hewlett and Walmley, 2002). In the process of laser ablation, the single pulse-width has great influence in the threshold energy of the photoablation effect (Kurtz *et al*., 1997). Juhasz *et al*. (1999) compared ultrashort pulsed laser technology in corneal refractive surgery with longer pulse-width nanosecond or picosecond's laser pulses, femtosecond laser-tissue interactions occurs with significantly smaller threshold energy, which means a much less amount of energy is delivered to the corneal surface by single pulse and less tissue is removed.

At present, the ultrashort pulse-width laser devices marketed can achieve the pulse width duration to a few hundreds Fs level. The rapid switching of DMD has completely reached the requirement of ultrashort pulsed laser devices and guarantees a higher precision.

ii) High resolution and unlimited beam shaping ability

The existing researches on relation of scanning laser beam size and ablation result has proved that smaller beam size has better effect in eliminating higher order aberrations and achieving higher surgical precision. The performance of traditional laser refractive surgery is limited by the fixed minimum laser beam size and shape; only fixed-sizes or shapes (scanning and broad-beam ablation) are provided for different individual cases. And because of the consideration of shortening the surgical period, applying an infinitely small laser beam to remove all vision errors is impossible in practice. The DMD technology provides a magnificent solution for the problem. The resolution of a DMD panel is decided by the size of the micro-mirror element, which is only 17 μm or less. When it is working on reflecting mode, the selected units reflect the incident laser beam to the target area, as displayed in Figure 6.11. Because each micro-mirror on the panel is controllable, reflection of irregular shape and unconnected image can also be implemented, which can be used to correct partial corneal curvature while the ablation on other area is processing. This function works like the multi-spots technique but with a much higher flexibility.

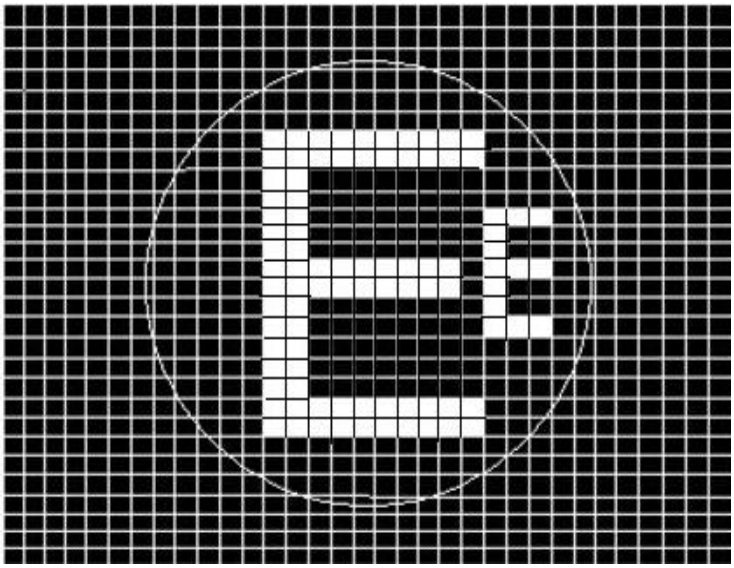

Figure 6.11 A DMD panel working on reflecting mode, the circle stands for the diameter of the laser beam.

In Figure 6.11, the circle stands for the diameter of an incident laser beam. The dark grids stand for micro-mirrors that are in the "off" mode. Laser energy projected on the dark area is diffusing reflected and will not arrive at the target surface. The bright E pattern is comprised of micro-mirrors that are in the "on" mode. This part of energy is delivered to the target area with the shape of the letter E.

iii) Low absorption of heat

Working on reflecting mode, the micro-mirrors absorb only negligible amount of heat from the illuminating laser resource, while more than 86% of the incident energy is delivered to the target (Hewlett and Walmley, 2002), which guarantees the transfer rate and prevents the system from overheating.

6.3 Concept of a refractive surgery system adopting digital mirror device as the beam shaping and delivery subsystem

The instrumentation for laser refractive surgeries typically consists of an argon-fluoride excimer laser (193 *nm*), beam shaping devices and a system delivering the laser beam to the human cornea (Esperance *et al*., 1989; Forster *et al*., 1993).

Beam shaping function of traditional broad beam laser is controlled by motorized iris (for myopia and hyperopia) and motorized slit (for astigmatism) based on profile calculated by the Munnerlyn formula (Forster *et al*., 1993). In recent years, complex scanning beam-delivery system was adopted to improve the surgical precision. With control of a small laser spot, different part of the corneal can be etched independently to realize more particular ablation profile. However, there are a number of problematic issues with the current scanning spot systems.

First is the operation time. According to Manns's method, the ideal ablation time can be calculated by the ratio of the total amount of removal and single pulse ablation volume. Using a smaller spot for higher ablation precision will definitely extend the surgical duration. Longer time is consumed for laser beam scanning over the corneal surface. However, the change of hydration of cornea by time may cause obvious variation of ablation rate (Mrochen *et al*., 2000; Anderson *et al*., 2004).

Second is the difficulty of laser delivery. Scanning laser systems require extremely accurate spot locating to deliver the particular ablation profile and achieve necessary spot overlap. The influence of decentration brings significantly larger error to the procedures comparing to surgeries using broad beam laser. High-frequency eye trackers are required to reduce the error induced by eye movement during the surgery (Bueeler and Mrochen, 2004; Bueeler and Mrochen, 2005).

Third is the corneal roughness. The necessary overlap of laser spots trends to create corneal roughness in the ablation result since the ablation depth of overlapping area is multipled.

System for comprehensive wavefront aberration correction.

A refractive surgery system utilizing digital mirror devices (DMD) as the beam shaping and delivery subsystem is sketched, which can theoretically overcome the above limitations. The system diagram is displayed in Figure 6.12. It consists of a 193 *nm* UV laser source, beam shaping optics, a DMD beam shaping and delivery system, a double wavelength beam splitter, a high-frequency eye tracker and a real-time wavefront sensing system.

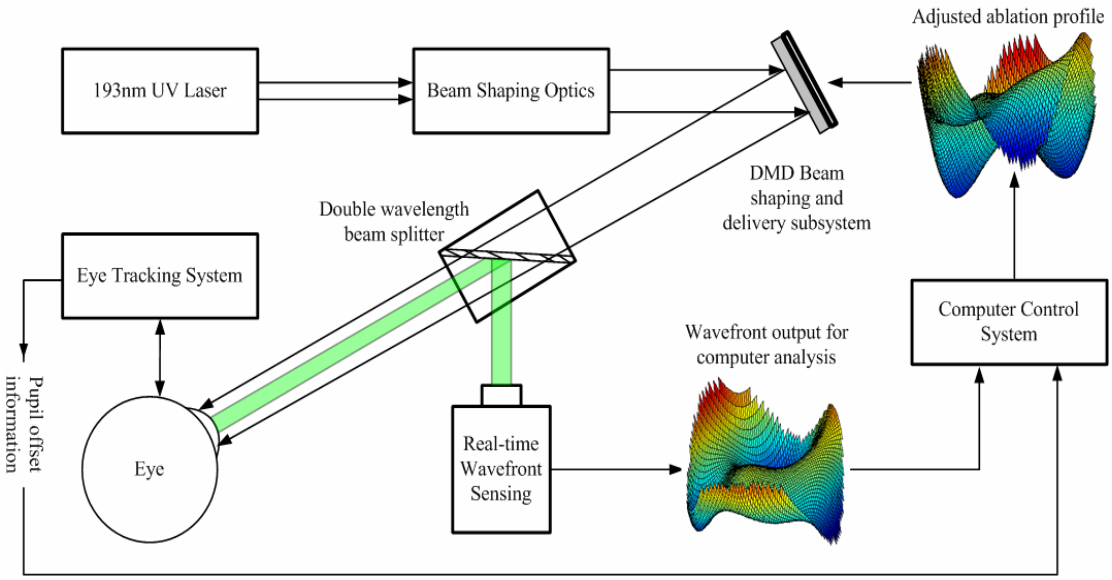

Figure 6.12 Proposed wavefront based refractive surgery system with the beam shaping and delivery subsystem utilizing DMD.

All the components are connected to a computer control system. The operation of the system will be described in details.

i) 193 nm UV Laser source

During the operation, the laser system is emitting an excimer laser working at 193 *nm* wavelength, which has a flat-hat profile and is suitable for common broad beam refractive surgery.

ii) Beam shaping optics

The laser beam is then passing the beam shaping optics, which consist of depolarization filters (Jimenez *et al*., 2004) and a set of extender lens enlarging the diameter of the original laser to exactly cover the whole ablation zone.

iii) DMD beam shaping and delivery system

The extended beam then arrives at the DMD (Texas Instruments). Based on the pre-calculated ablation profile from wavefront aberrations, plusing the additional compensation by Equation (6-12), a real ablation pattern is obtained. According to the required ablation depth of each point (ρ, θ) on the cornea, a new ablation pulse distribution map is calculated by simply dividing the ablation depth per pulse.

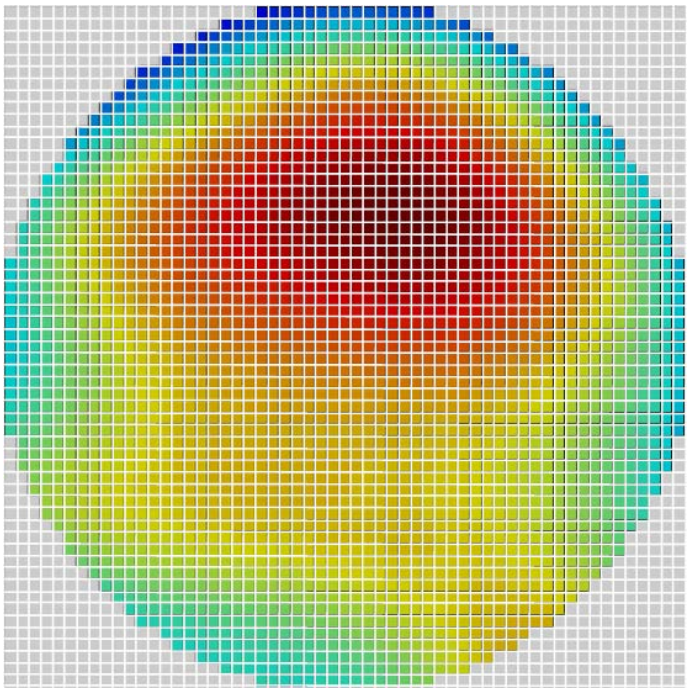

Figure 6.13 DMD beam shaping for a pre-calculated ablation profile from wavefront.

As shown in Figure 6.13, the area with warmer color indicates a larger number of pulses required, each grid in the graph includes 10×10 micro mirrors. The related micro-mirrors on the DMD panel keep the "on" state until required number of pulses is delivered. The illumination period is calculated by the ratio of desired pulses and repetition rate.

iv) Eye tracking system

High-frequency eye trackers are most necessary for scanning laser surgery due to the accuracy requirement of spot locating. The latency of eye trackers was reported to have obvious impact on the surgery outcome (Bueeler and Mrochen, 2005). One set of eye tracking system is adopted in this surgery system model to capture real-time information of eye movement during the surgery. The data of pupil decentration is transferred to the computer control system, which will adjust the beam delivery direction.

v) Real-time wavefront sensing system

A wavefront sensor using visible laser (555 *nm*) is adopted to monitor the eye's wavefront aberration. It is inserted to the optical path by using a dual wavelength

beam splitter. The wavefront feedback is also sent to the computer control system for adjusting the ablation profile in a dynamic condition.

Advantages of the proposed system are evident. By using the DMD beam shaping and delivery system, the whole ablation pattern is delivered at the same time, which can significantly shorten the ablation period. Therefore, a lower repetition rate can be adopted to avoid local heating (Ishihara *et al*., 2002). Moreover, the requirement of accurate eye-tracker is also simplified when the whole ablation zone is treated at the same time. As shown in the study of simulated decentered ablation in Chapter 5, a 150 μm one-way decentration brings obvious effect on postoperative HOA wavefront RMS comparing to the ideal situation with no VK pupil offset. However, the total wavefront RMS drops to only 8.5% of the preoperative value. A modern high frequency eye tracker with latency smaller than 5ms can significantly reduce the influence of decentration. The introduction of real-time wavefront sensor provides a strong aid to monitor the change in wavefront, which can avoid the error produced by change of corneal hydration and other unexpected situations.

Chapter 7

Conclusions and Recommendations

7.1 Summary of the present study

The optimization of LASIK procedures is a complicated problem, due to the interaction of technological and pathologic factors. The aim of this research study was to develop the methodology to improve the current LASIK technology to achieve a higher surgical precision, thereby to reduce the risk of possible post-operative symptom.

In this study, the latest technological developments of both algorithms and hardware, which can be applied to improve the LASIK procedures, have been investigated. The principal contributions and conclusions of the present research are summarized below:

1) A computerized simulation program of corneal ablation process based on a wavefront-only ablation profile method has first been developed. Unlike the other reported simulation based on theoretical human eye models, the presented methodology utilized topographic and wavefront data from a group of real patients, which are all suitable candidates for LASIK treatment. Therefore, it provides a much better connection with clinical practice. The developed methodology can also be used as a screening tool to predict patient's visual improvement before surgery.

2) As examined by the computer simulation, wavefront-only corneal ablation algorithms could potentially lead to significantly better visual outcomes than those normally encountered in untreated emmetropes. Small amount of alignment error during surgery, (<150 μm as examined), does not bring significant changes to surgical outcome if a small laser beam is used. However, alignment error in standard surgery procedures must be limited.

3) By combining the advantages of wavefront-optimized ablation algorithms, high-precision laser delivery methods and real-time beam shaping technologies, refractive surgery for comprehensive vision improvement is theoretically achievable.

7.2 Recommendation for future work

The main objective of this research study is to develop the methodology to improve the performance of LASIK procedures. Although the present study has enhanced the knowledge in this area while covering most of the technological factors, the following tasks need to be further considered in future studies:

1) To examine the efficiency of wavefront-only ablation algorithms, experiments on subjects with a large pupil size (>6 *mm*) and higher amount of correction as well as patients with unsuccessful previous refractive surgeries can help to investigate the application on extended cases.

2) The developed computer simulation of corneal ablation process used an ideal laser beam. Investigation of ablation using a finite laser beam size will provide more connection to current LASIK technology.

3) The present study does not consider the factors of biological changes of the human ocular before, during and after the surgery, which requires the eye model with an extremely high precision. It would be a valuable area for further research in this field.

Reference

Alessio G, Boscia F, La-Tegola MG and Sborgia C (2001). "Topography-driven excimer laser for the retreatment of decentralized myopic photorefractive keratectomy." Ophthamology **108**: 1695-1703.

Alio JL, Belda JI, Osman AA and Shalaby AMM (2003). "Topography-guided laser in situ keratomileusis (TOPOLINK) to correct irregular astgmatism after previous refractive surgery." J Cataract Refract Surg **19**: 516-527.

Al-qahtani JM, Mclean IW, Weiblinger RP and Ediger MN (2001). "Preliminary in vitro study of the histological effects of low fluence 193-nm excimer laser irradiation of corneal tissue." J Refract Surg **17**: 105-109.

Anderson I, Sanders DR, Saarloos PV and Ardrey-IV WJ (2004). "Treatment of irregular astigmatism with a 213 nm solid-state, diode-pumped neodymium: YAG ablative laser." J Cataract Refract Surg **30**: 2145-2151.

Anera RG, Jimenez JR, Jimenez del B and Hita E (2003). "Changes in corneal asphericity after laser reflection losses and nonnormal incidence upon the anterior cornea." Opt Letter **28**: 417-419.

Applegate RA, Sarver EJ and Khemsara V (2002). "Are all aberrations equal?" J Refract Surg **18**: S556-S562.

Applegate RA, Thibos LN and Himantel G (2001). "Optics of aberroscopy and super vision." J Cataract Refract Surg **27**: 1093-1107.

Artal P and Guirao A (1998). "Contribution of the cornea and the lens to the aberrations of the human eye." J Cataract Refract Surg **23**(21): 1713-1715.

Bailey MD and Mitchell GL (2001). "Patient satisfaction and visual symptoms after laser in situ keratomileusis." Ophthamology **110**(7): 1371-1378.

Balazsi G, Mullie M, Lasswell L, Lee PA and Duh YJ (2001). "Laser in situ keratomileusis with a scanning excimer laser for the correction of low to moderate myopia with and without astigmatism." J Cataract Refract Surg **27**: 1942-1951.

Brown SM and Campbell CE (2003). "Systematic underablation in laser in situ keratomileusis: Ablation pattern identified by advanced topographical analysis." J Cataract Refract Surg **29**: 1621-1625.

Brunette I, Gresset J and Boivin JF (2000). "Functional outcome and satisfaction after photorefractive keratectomy. Part 2: survey of 690 patients; the Canadian Refractive Surgery Research Group." Ophthamology **107**: 1790-1796.

Bueeler M and Mrochen M (2004). "Limitations of pupil tracking in refractive surgery: system error in determination of corneal locations." J Refract Surg **20**: 371-378.

Bueeler M and Mrochen M (2005). "Simulation of eye-tracker latency, spot size, and ablation pulse depth on the correction of high order wavefront aberrations with scanning spot laser systems." J Refract Surg **21**: 38-47.

Bueeler M, Mrochen M and Seiler T (2003). "Maximum permissible lateral decentration in aberration-sensing and wavefront-guided corneal ablation." J Cataract Refract Surg **29**: 257-263.

Buzard KA and Fundingsland BR (1997). "Treatment of irregular astigmatism with a broad beam excimer laser." J Refract Surg **13**: 624-636.

Campbell FW and Green DG (1965). "Optical and retinal factors affecting visual resolution." J Physiol **181**(5): 76-93.

Chang AW, Tsang AC, Contreras JE, Huynh PD, Calvano CJ, Crnic-Rein TC and Thall EH (2003). "Corneal tissue ablation depth and the Munnerlyn formula." J Cataract Refract Surg **29**: 1204-1210.

Cheng X, Bradley A and Thibos LN (2004). "Predicting sbjective judgement of best focus with objective image quality metrics." Journal of Vision **4**: 310-321.

Chuck RS, Behrens A, Wellik SR, Liaw LH, Sweet PM, Osann KE, McDonnell PJ and Berns MW (2001). "Simple organ cornea culture model for re-epithelialization after in vitro excimer laser ablation." Laser in Surgery and Medicine **29**: 288-292.

Collins MJ, Davis B and Wood J (1995). "Microfluctuations of steady-state accommodation and the cardiopulmonary system." Vis Res **35**: 2491-2502.

Courville CB, Smolek MK and Klyce SD (2003). "Contribution of the ocular surface to visual optics." Experimental Eye Research(78): 417-425.

Dausch D, Schroder E and Dausch S (2000). "Topography-controlled excimer laser photorefractive keratectomy." J Refract Surg **16**: 13-22.

Dave T (1998). "Current developments in measurement of corneal topograpgy." Contact Lens and Anterior Eye **21**: S13-S30.

Donnenfeld E (2004). "The pupil is a moving target: centration, repeatability, and registration." J Cataract Refract Surg **20**: S593-S596.

Doss JD, Hutson RL, Rowsey JJ and Brown DR (1981). "Method for calculation of corneal profile and power distribution." Arch Ophthalmol **99**: 1261-1265.

Erie JC, Hodge DO and Bourne WM (2004). "Confocal microscopy evaluation of stromal ablation depth after myopic laser in situ keratomileusis and photorefractive keratectomy." J Cataract Refract Surg **30**: 321-325.

Esperance FAL, Warner JW, Telfair WB, Yoder PR and Martin CA (1989). "Excimer laser instrumentation and technique for human corneal surgery." Arch Ophthalmol **107**: 131-139.

Fernandez GET and Serrano MG (2000). "Early clinical experience using custom excimer laser ablations to treat irregular astigmatism." J Cataract Refract Surg **26**: 1442-1450.

Fiore T, Carones F and Brancato R (2001). "Broad beam vs. flying spot excimer laser: refractive and videokeratographic outcomes of two different ablation profiles after photorefractive keratectomy." J Refract Surg **17**: 534-541.

Fogla R and Rao SK (2000). "Pupillometry using videokeratography in eyes with dark brown irides." J Cataract Refract Surg **26**: 1266-1267.

Forster W, Beck R and Busse H (1993). "Design and development of a new 193-nanometer excimer laser surgical system." Refractive Corneal Surg **9**: 293-299.

Gatinel D, Hoang XT and Azar DT (2002). "Volume estimation of excimer laser tissue ablation for correction of spherical myopia and hyperopia." Invest Ophthalmol Vis Sci **43**(5): 1445-1449.

Gibralter R and Trokel SL (1994). "Correction of irregular astigmatism with the excimer laser." Ophthamology **101**: 1310-1315.

Ginis HS, Katsanevaki VJ and Pallikaris IG (2003). "Influence of ablation parameters on refractive changes after phototherapeutic keratectomy." J Refract Surg **19**: 443-448.

Guell JL and Muller A (1996). "Laser in situ keratomileusis (LASIK) for myopia from -7 to -18 diopters." J Refract Surg **12**: 222-228.

Guirao A and Artal P (2000). "Corneal wave aberration from videokeratography accuracy and limitations of the procedure." J Opt Soc Am A **17**(6): 955-965.

Guirao A, Williams DR and Cox IG (2000). "Effect of rotation and translation on the expected benefit of an ideal method to correct the eye's higher-order aberrations." J Opt Soc Am A **18**: 1003-1015.

Guirao A, Williams DR and MacRae SM (2003). "Effect of beam size on the expected benefit of customized laser refractive surgery." J Cataract Refract Surg **19**: 15-23.

Hewlett WE and Walmley B (2002). Programmable light beam shape altering device using programmable micromirrors. 6,421,165 B2 ,US, Light & Sound Design Ltd.

Holladay JT (2002). "The high cost of inaccurate pupillometry." Rev Ophthal **9**: 47-49.

Homolka P, Biowski R, Kaminski S, Barisani T, Husinsky W, Bergmann H and Grabner G (1999). "Laser reshaping of corneal transplants in vitro: area ablation with small overlapping laser spots produced by a pulsed scanning laser beam using an optimizing ablation algorithm." Phys. Med. Biol. **44**: 1169-1180.

Huang D (2002). "Spot size and quality of scanning laser correction of higher-order wavefront aberration." J Cataract Refract Surg **28**: 407-416.

Huang D, Tang M and Shekhar R (2003). "Mathematical model of corneal surface smoothing after laser refractive surgery." Am J Ophthalmol **135**: 267-278.

Iseli HP, Mrochen M, Hafezi F and Seiler T (2004). "Clinical photoablation with a 500-Hz scanning spot excimer laser." J Cataract Refract Surg **20**: 831-834.

Ishihara M, Arai T, Sato S, Morimoto Y, Obara M and Kikuchi M (2002). "Measurement of the surface temperature of the cornea during ArF excimer laser ablation by thermal radiometry with a 15-nanosecond time response." Laser in Surgery and Medicine **30**: 54-59.

Iskander DR, Collins MJ and Davis B (2001). "Optimal modeling of corneal surfaces with Zernike polinomials." IEEE Trans on Biomed Eng **48**(1): 87-95.

Iskander DR, Collins MJ, Morelande MR and Zhu M (2004). "Analyzing the dynamic wavefront aberrations in the human eye." IEEE Trans on Biomed Eng **51**: 1969-1980.

Jimenez JR, Anera RG and Barco LJD (2001). "Effect on visual function of approximations of the corneal-ablation profile during refractive surgery." Appl Opt **40**: 2200-2205.

Jimenez JR, Anera RG and Barco LJD (2004). "Influence of laser polarization on ocular refractive parameters after refractive surgery." Opt Letter **29**: 962-965.

Jimenez JR, Anera RG, Jimenez del BL and Hita E (2002). "Effect on laser-ablation algorithms of reflection losses and nonnormal incidence on the anterior cornea." Appl Phys letter **81**(8).

Jimenez JR, Anera RG, Barco LJD, Hita E and Perez-Ocon F (2005). "Correction factor for ablation algorithms used in corneal refractive surgery with gaussian-profile beams." J Opt Soc Am **13**: 336-343.

Juhasz T, Loesel F H, Kurtz R M, Horvath C, Bille J F and Mourou G A (1999). "Corneal refractive surgery with femtosecond laser." IEEE Journal of selected topics in quantum electronics **5**(4): 902-910.

Klein SA (1998). "Optimal corneal ablation for eyes with arbitrary Hartmann-Shack aberrations." J Opt Soc Am A **15**(9): 2580-2588.

Knorz MC and Jendritza B (2000). "Topographically-guided laser in situ keratomileusis to treat corneal irregularities." Ophthamology **107**: 1138-1143.

Kohnen T (2004). "Combining wavefront and topography data for excimer laser surgery: The future of customized ablation?" J Cataract Refract Surg **30**: 285-286.

Komazaki I and Y E (2003). Optical displacement sensor having a semiconductor laser light source using an optical element which can control beam angle and beam shape. US 6,631,005 B1, Olympus Optical Co., Ltd.

Krueger RR and Trokel SL (1985). "Quantitation of corneal ablation by ultraviolet laser light." Arch Ophthalmol **103**: 1741-1742.

Kurtz RM, Liu XB, Elner VM, Squier JA, Du DT and Mourou GA (1997). "Photodisruption in the human cornea as a function of laser pulse width." J Refract Surg **13**: 653-658.

Lawless MA and Hodge C (2005). "Wavefront's role in corneal refractive surgery." Clinical and Experiment Ophthalmology **33**: 199-209.

Lee YC, Hu FR and Wang IJ (2003). "Quality of vision after laser in situ keratomileusis Influence of dioptric correction and pupil size on visual function." J Cataract Refract Surg **29**: 769-777.

Li ZJ and Zhu CH (2001). Laser Biomedical Engineering. Wuhan, PRC, Huazhong University of Science and Technology Press.

Liang J, Grimm B, Goelz S and Bille JF (1994). "Objective measurement of wave aberrations of the human eye with the use of a Hartmann-Shack wave-front sensor." J Opt Soc Am A **11**: 1949-1957.

MacRae SM, Schwiegerling J and Snyder R (2000). "Customized corneal ablation and super vision." J Refract Surg **16**: S230-S235.

Macrcos S, Barbero S, Llorente L and Merayo-Lloves J (2001). "Optical response to Lasik surgery for myopia from total and corneal aberration measurements." Invest Ophthalmol Vis Sci **42**(13): 3349-3356.

Mahajan VN (1998). Optical Imagine and Aberrations, SPIE Optical Engineering Press.

Manns F, Ho A, Parel JM and Culbertson W (2002). "Ablation profiles for wavefront-guided correction of myopia and primary spherical aberration." J Cataract Refract Surg **28**: 766-774.

Manns F, Shen J H, Soderberg P, Matsui T and Parel JM (1995). "Development of an algorithm for corneal reshaping with a scanning laser beam." Appl Opt **34**(21): 4600-4608.

Marcos S, Cano D and Barbero S (2003). "Increase in corneal asphericity after standard laser insitu keratomileusis for myopia is not inherent to the Munnerlyn algorithm." J Refract Surg **19**: S592-S596.

Marsack JD, Thibos LN and Applegate RA (2004). "Metrics of optical quality derived from wave aberrations predict visual performance." Journal of Vision **4**: 322-328.

Mattioli R and Tripoli NK (1997). "Corneal geometry reconstruction with the Keratron videokeratographer." Optometry and Vision Science **14**: 881-894.

McGhee CNJ, Craig JP and Sachdev N (2000). "Functional, psychological, and satisfaction outcomes of laser in situ keratomileusis for high myopia." J Cataract Refract Surg **26**(497-509).

Miller AE, McCulley JP and Bowman RW (2001). "Patient satisfaction after LASIK for myopia." CLAO J **27**: 84-88.

Moreno B and Navarro R (2000). "Laser ray-tracing versus Hartmann-Shack sensor for measuring optical aberrations in the human eye." J Opt Soc Am A **17**: 1-14.

Mrochen M, Bueeler M, Iseli HP, Hafezi F and Seiler T (2004 a). "Transfering wavefront measurement into corneal ablations: An overview of related topics." J Refract Surg **20**: S550-S554.

Mrochen M, Donitzky C, Wullner C and Loffler J (2004 b). "Wavefront-optimized ablation profiles: Theoretical background." J Cataract Refract Surg **30**: 775-785.

Mrochen M, Jankov M, Bueeler M and Seiler T (2003). "Correlation between corneal and total wavefront aberrations in myopic eyes." J Cataract Refract Surg **19**(2): 104-112.

Mrochen M, Karmmerer M, Mierdel P and Seiler T (2001). "Increased higher-order optical aberrations after laser refractive surgery: A problem of subclinical decentration." J Cataract Refract Surg **27**: 362-369.

Mrochen M, Ronald RK, Bueeler M and Seiler T (2002). "Aberration-sensing and wavefront-guided laser insitu keratomileusis: Management of Decentered Ablation." J Cataract Refract Surg **18**: 418-429.

Mrochen M and Seiler T (2001). "Influence of corneal curvature on calculation of ablation patterns used in photorefractive surgery." J Cataract Refract Surg **17**: S585-S584.

Mrochen M, Semshichen V, Funk RHW and Seiler T (2000). "Limitations of Erbium: YAG laser photorefractive keratectomy." J Refract Surg **16**: 51-59.

Munnerlyn CR, Koons SJ and Marshall J (1988). "Photorefractive keratectomy: a technique for laser refractive surgery." J Cataract Refract Surg **14**: 46-52.

Navarro R, Santamaria J and Bescos J (1985). "Accommodation dependent model of the human eye with aspherics." J Opt Soc Am A **2**: 1273-1281.

Pallikaris IG, Kymionis GD, Panagopoulou SI, Siganos CS, Theodorakis MA and Pallikaris AI (2002). "Induced optical aberrations following formation of a laser in situ keratomileusis flap." J Cataract Refract Surg **28**: 1737-1741.

Rand RH, Howland HC and Applegate RA (1997). "Mathematical model of a Placido disk keratometer and its implications for recovery of corneal topography." Optometry and Vision Science **74**: 926-930.

Roberts C (2000). "Future challenges to aberration-free ablative procedures." J Refract Surg **16**: S623-S629

Salmon TO and Thibos LN (2002). "Videokeratoscope-line-of-sight misalignment and its effect on measurements of corneal and internal ocular aberrations." J Opt Soc Am A **19**: 657-669.

Schwiegerling J and Greivenkamp JE (1997). "Using corneal height maps and polynomial decomposition to determine corneal aberrations." Optometry and Vision Science **74**: 906-916.

Scisco A, Hull CC, Stephenson CG, Baldwin H, O'Bratt D and Marshall J (2003). "Fourier analysis of induced irregular astigmatism." J Cataract Refract Surg **29**: 457-461.

Seitz B, Langenbucher Achim, Kus MM and Harrer M (1998). "Experimental correction of irregular corneal astigmatism using topography-based flying-spot-mode excimer laser photoablation." Am J Ophthalmol **125**: 252-256.

Shimmick JK (2001). "The VISX perspective on fixed vs. variable spot scanning ablation." J Refract Surg **17**: 594-595.

Shimmick JK, Telfair WB, Munnerlyn CR, Bartlett JD and Trokel SL (1997). "Corneal ablation profilometry and steep central island." J Refract Surg **13**: 235-245.

Stiles WS and Crawford BH (1933). "The luminous efficiency of rays entering the pupil at different points." Proc R Soc B **112**: 428-450.

Sun C W, Lu Q S, Fan Z X, Chen Y Z, Li C F, Guan J L and Guan C W (2002). Laser Radiation Effect. Beijing, PRC, Nation Defence Industry Press.

Terry K (2000). Lasik Vision Correction. Ohio, USA, Group of Medical Management Service, Med World Publishing.

Thibos LN, Hong X, Bradley A and Applegate RA (2004). "Accuracy and precision of objective refraction from wavefront aberrations." Journal of Vision **4**: 329-351.

Vetrugno M, Maino A, Valenzano E and Cardia L (2001). "Corneal temperature changes during photorefractive keratectomy using the laserscan 2000 flying spot laser." J Refract Surg **17**: 454-459.

Wachler BSB and Krueger RR (2000). "Agreement and repeatability of pupillometry using videokeratography and infrared devices." J Cataract Refract Surg **26**: 35-40.

Wiesinger-Jendritza B, Knorz MC, Hugger P and Liermann A (1998). "Laser in situ keratomileusis assisted by corneal topography." J Cataract Refract Surg **24**: 166-174.

Williams RE, Freeman JF and Freeman MJ (2002). Laser eye surgery system using wavefront sensor analysis to control digital micromirror device (DMD) mirror patterns. No. US 6,394,999, US, Memphis Eye & Cataract Associates Ambulatory Surgery Center.

Wyant JC and Creath K (1992). Basic wavefront aberration theory for optical metrology. Applied Optics and optical engineering, Academic Press, Inc. **11**.

Xu GD (1995). Ophthalmology Dioptrics. Beijing, PRC, Military Medical Science Press.

Yang KC (2000). Laser principle and technology. Wuhan, China, Huazhong University of Science and Technology Press.

Zhang YM (1977). Applied Optrics. Tianjin, China, National Defence Industrial Press.

Appendix 1. Concept of a wavefront based refractive surgery system with the beam shaping and delivery subsystem utilizing DMD.